Urban Climate 64 (2025) 102717

Contents lists available at ScienceDirect

Urban Climate

journal homepage: www.elsevier.com/locate/uclim

# A multi-city statistical modelling of surface urban heat island: Application to Italian cities

Antonio Esposito [a,b], Gianluca Pappaccogli [b,*], Fabio Bozzeda [b,c], Riccardo Buccolieri [b,d]

[a] Department of Mathematics and Physics, University of Salento, Via per Arnesano, snc, 73100 Lecce, Italy
[b] Department of Biological and Environmental Sciences and Technologies, University of Salento, S.P. 6 Lecce-Monteroni, 73100 Lecce, Italy
[c] National Biodiversity Future Center (NBFC), Palermo, Italy
[d] Institute of Atmospheric Sciences and Climate (ISAC), National Research Council (CNR), Str. prov. Lecce-Monteroni, Km 1,2, 73100 Lecce, Italy

A R T I C L E I N F O

*Keywords:*
SUHII
Remote sensing
Sentinel-3 satellite
Urban morphology
Multiple linear regression
Italian cities

A B S T R A C T

Surface urban heat island intensity (SUHII) is a key indicator of thermal patterns in urban environments, determined by complex interactions between land use, morphology and climate conditions. This study presents and applies a predictive framework to assess SUHII in four Italian cities (Lecce, Bari, Milan and Turin) using satellite data of land surface temperature (LST), urban morphological parameters and advanced statistical modelling. More than 1000 Sentinel-3 images of summer periods (June, July and August) for the years 2022 and 2023 were processed to assess daytime and nighttime SUHII. Multiple linear regression analyses, supported by variance inflation factor (VIF) filtering and residuals diagnostics, revealed that impervious surface fraction (ISF), leaf area index (LAI) and albedo were the most influential predictors. The results showed significant spatial and temporal variability in SUHII, with Milan and Turin showing pronounced heat accumulation, especially at night, while Lecce and Bari showed lower or negative diurnal SUHII. Generalized regression models were developed based on multidimensional scaling (MDS) and SIMPER analysis. Scenario testing in Milan indicated that increasing LAI and surface albedo can reduce SUHII by up to 1 °C. The proposed statistical model is scalable, computationally efficient and well-suited for urban-scale applications, making it a practical tool for mapping and analyzing SUHII patterns in diverse city contexts.

## 1. Introduction

Urban areas are increasingly exposed to climate-related risks, particularly extreme heat, as a result of ongoing global warming and rapid urbanization (IPCC, 2022). These conditions have intensified the need for reliable tools to analyze and monitor urban microclimates, given their direct impact on public health (Rydin et al., 2012), energy demand (Pappaccogli et al., 2020, 2021; Santamouris et al., 2015), and air quality (Martilli et al., 2021). These impacts highlight the growing urgency to better understand and quantify urban thermal environments. However, despite extensive research on the urban heat island (UHI) phenomenon, there is still a lack of reliable and standardized analytical tools capable of capturing the spatial complexity of urban microclimates. Filling this gap is essential for developing evidence-based approaches to assess and manage heat-related risks in cities (Mirzaei and Haghighat, 2010;

* Corresponding author.
*E-mail address:* gianluca.pappaccogli@unisalento.it (G. Pappaccogli).

https://doi.org/10.1016/j.uclim.2025.102717
Received 21 July 2025; Received in revised form 4 November 2025; Accepted 21 November 2025
Available online 27 November 2025

Roy et al., 2025).

Urban climate research has traditionally relied on in situ air temperature data collected by ground-based weather stations to quantify the UHI effect (Donateo et al., 2023). Although these measurements provide accurate temporal information, the spatial heterogeneity of urban environments often exceeds the representativeness of point observations (Heaviside et al., 2017). To overcome these limitations, satellite remote sensing has become a key tool, capable of providing spatially continuous observations of surface characteristics (Albini et al., 2025; Zhang et al., 2022a, 2022b). In particular, land surface temperature (LST) derived from thermal infrared sensors provides a direct indicator of energy exchange between the surface and the atmosphere and is recognized as an essential climate variable (ECV) by the World Meteorological Organization (WMO, 2025). Urban warming derived from satellite LST, known as the surface urban heat island (SUHI), has therefore become a focal point in urban climate studies (Zhou et al., 2019; Clinton and Gong, 2013).

To interpret SUHI dynamics, researchers have widely used land use/land cover (LULC) data and spectral indices such as the normalized difference vegetation index (NDVI), normalized difference built-up index (NDBI), and normalized difference water index (NDWI). These indicators capture the biophysical and morphological properties of urban surfaces and help explain local variations in LST (Esposito et al., 2024; Garzón et al., 2021; Shi et al., 2019;). However, most studies have analysed these relationships independently or through simple correlation analyses, without quantifying the relative contribution of each variable to temperature variability. Furthermore, despite significant advances in data availability and processing techniques, there is still no standardized, transferable analytical framework capable of capturing the spatial complexity of urban microclimates and the combined influence of morphological, radiative, and biophysical factors. This limitation hinders the comparison of cities with different climatic and morphological conditions and the derivation of generalizable insights for urban climate assessment. Multiple Linear Regression (MLR) models offer a powerful approach for disentangling the complex relationships between surface temperature and urban characteristics (Garzón et al., 2021). By estimating the weighted influence of multiple independent variables, MLR enables a more comprehensive understanding of how specific features, such as vegetation cover, surface albedo, impervious fraction, or building height drive urban thermal patterns (Zheng et al., 2021; Deng et al., 2021; Schwarz et al., 2012). Recent studies have demonstrated the potential of MLR approaches to quantify the contribution of urban morphological factors and vegetation to surface temperature variability (e.g., Oukawa et al., 2022; Garzón et al., 2021; Zheng et al., 2021; Deng et al., 2021). However, most applications remain limited to city-scale analyses or specific climatic regions, often relying on a restricted set of explanatory variables and lacking cross-comparative consistency. Moreover, few studies have explored the integration of radiative, structural, and thermal parameters within a standardized and widely applicable regression framework. Addressing these limitations, the present study aims to develop a standardized and

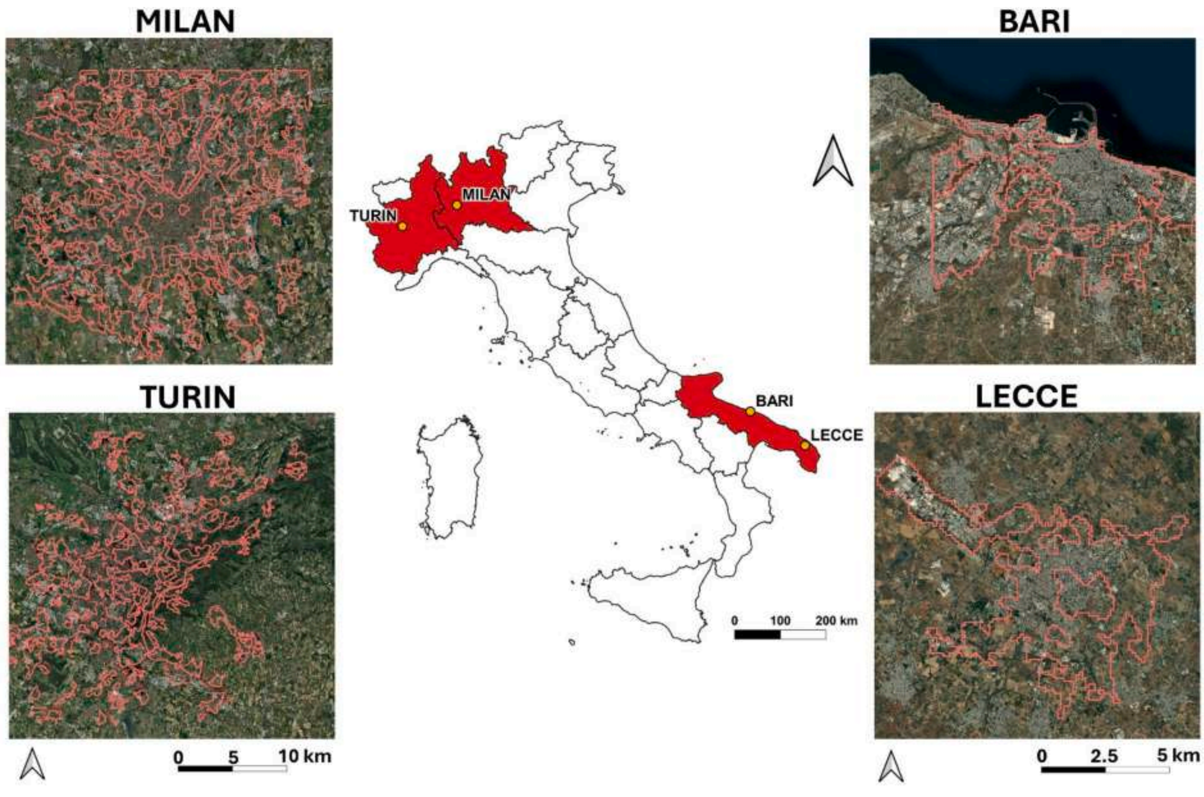


**Fig. 1.** Location of selected cities (their regions colored red). Satellite images of the Italian cities investigated (base maps from Google Earth Pro). Contour lines represent the boundaries of the three main Corine Land Cover classes (CLC 1, 2,3) considered in this study. (For interpretation of the references to colour in this figure legend, the reader is referred to the web version of this article.)

interpretable MLR model capable of assessing the intensity of the urban heat island effect under varying urban and climatic conditions.

A major limitation in the current literature is the lack of standardized, transferable methods that can quantify the impact of urban form and surface properties on SUHI intensity, while also being practical for policy-oriented applications. Moreover, few studies combine morphological, radiative, and thermal descriptors using a consistent and scalable framework that can be applied across different cities. (Deilami et al., 2018).

The primary objective of this study is to develop a MLR model for estimating SUHI intensity by explicitly accounting for detailed urban morphological and biophysical characteristics. The aim is to provide a simple yet effective analytical tool to evaluate the potential impact of mitigation strategies, such as increasing vegetation or altering surface radiative properties on urban LST.

To this end, the proposed model integrates satellite-derived surface temperature data with a set of globally and regionally available indicators representing key aspects of urban form and surface properties, including land cover, building structure, impervious surfaces, albedo and vegetation. Collectively, these parameters capture the radiative, structural, and biophysical characteristics that drive spatial variability in surface urban heat intensity. This conceptual framework supports the subsequent statistical analysis, which aims to identify the urban characteristics that most strongly influence SUHI intensity.A preliminary statistical analysis was conducted to determine which of these urban features most significantly influence SUHI intensity. The most relevant factors were then selected and incorporated into the MLR model. Rather than predicting exact temperatures, the model functions as an analytical framework for estimating how variations in urban characteristics, such as increased vegetation or higher albedo may reduce LST and SUHI intensity.

The proposed model is adaptable to other urban areas with similar climatic conditions. By incorporating locally representative urban parameters, it enables the analysis of spatial thermal patterns and the evaluation of mitigation scenarios. The study introduces an innovative MLR framework that integrates radiative, structural, and thermal variables derived from open and standardized datasets. This approach provides a clear, practical, and computationally efficient tool for urban planners and policymakers to assess the impacts of climate adaptation strategies and support evidence-based urban climate planning.

## 2. Methodology

### 2.1. Description of the cities investigated

This study focuses on four Italian cities: the metropolitan areas of Bari, Milan and Turin, and the city of Lecce, included as representative of the University of Salento area. Lecce and Bari are characterized by a Mediterranean climate (Csa), with mild, wet winters and hot, dry summers, while Milan and Turin belong to the humid subtropical climate zone (Cfa), characterized by higher humidity and a more uniform distribution of rainfall.

The selected cities differ substantially in terms of urban structure and development history (Fig. 1). Milan is a large, compact metropolitan area with concentric urban expansion around a densely populated historic centre. Turin has a more extended and polycentric configuration, strongly influenced by major transport axes and industrial development. Lecce, on the other hand, is a medium-sized city with a low-density, predominantly residential urban fabric, surrounded by vast green and rural areas. Bari, in addition to being a coastal city, has a mixed configuration, with compact neighbourhoods inland and a more dispersed suburban expansion. The inclusion of these four cities captures a wide range of climatic and morphological conditions, from the highly urbanized metropolitan areas of the north to the more compact Mediterranean cities of the south. The morphological analysis conducted over the entire urban areas highlights that the four selected cities encompass a broad spectrum of urban geometries, ranging from compact, high-density configurations in Milan and Bari (characterized by greater building height and urban compactness) to more open, low-rise morphologies in Lecce and Turin (with wider street canyons and higher sky view factors). The results reveal a consistent gradient of urban form across the selected cases and underline how similar morphological patterns can occur under different climatic contexts, providing a meaningful combination of geometric and environmental conditions for comparative analysis.

### 2.2. Urban characteristics

Morphological and land use data for all cities were collected and analysed using shapefiles obtained from official institutional sources. Specifically:

- for Lecce and Bari, data were sourced from SIT Puglia (http://www.sit.puglia.it, accessed April 14, 2022)
- for Milan, data were sourced from the Milano Geoportale (https://geoportale.comune.milano.it, accessed June 17, 2022)
- for Turin, data were sourced from Geoportale Piemonte (https://geoportale.igr.piemonte.it/cms/, accessed on March 15, 2023)

Morphological analysis was conducted using QGIS software (version 3.22.1, https://www.qgis.org/en/site, accessed December 10, 2024). A region of interest was defined for each city, with dimensions appropriate to the urban scale. Specifically, a 10 km × 10 km area was selected for Lecce and Bari (hereafter referred to as "Lecce region" and "Bari region"), a 20 km × 20 km area for Milan ("Milan region"), and a 35 km × 35 km area for Turin ("Turin region").

The analysis involved key urban morphological parameters such as mean building height (HM), sky view factor (SVF), aspect ratio (AR), building surface fraction (BSF), impervious and permeable surface fractions (ISF and PSF). These parameters were calculated at a spatial resolution of 1 km following the classification framework proposed by Stewart and Oke (2012). This spatial resolution offers a robust and representative framework for characterizing neighborhood-scale urban processes, ensuring both computational efficiency and inter-city comparability, in line with the standards adopted by the Urban-PLUMBER protocol and widely recognized within the urban climate research community (Grimmond et al., 2010). For a full explanation of the calculation methodology, refer to Esposito et al., 2023, 2024 and Pappaccogli et al. (2025). In addition to the previously described morphological parameters, the analysis also included albedo (α), leaf area index (LAI), and shading (SHD).

The albedo was derived from Sentinel-3 OLCI data with an original spatial resolution of 300 m (https://cds.climate.copernicus.eu/datasets/satellite-albedo?tab=overview, accessed March 3, 2024), and then averaged over a 1 km resolution grid.

LAI was estimated using the normalized differential vegetation index (NDVI) obtained from Sentinel-3 images, applying the empirical relationship proposed by Saito et al. (2001):

$$\mathrm{LAI} = 0.57 \times \exp(2.33 \times \mathrm{NDVI}) \tag{1}$$

Finally, SHD was derived using a digital elevation model (DEM) and the "Shading" tool of QGIS, based on azimuth and solar altitude angles obtained from https://www.suncalc.org/, accessed March 3, 2025. Solar position data were collected at 30-min intervals between 8:00 a.m. and 10:00 a.m. during the summer months (June, July and August, hereafter JJA).

### 2.3. Satellite images and surface urban heat island (SUHI)

For the urban surface heat island intensity (SUHII) analysis, more than 1000 satellite images of LST were acquired for the four cities during JJA season. SUHII is defined as the difference between urban (LSTurb) and median rural temperatures (LSTrur):

$$\mathrm{SUHII} = \mathrm{LSTurb} - \mathrm{LSTrur} \tag{2}$$

The satellite images were obtained from the Level-2 LST product of the Sentinel-3 satellite (S3A and S3B), which provides daily thermal data for both daytime and nighttime (an average of 2–3 images between 8:00. and 10:00., and an average of 2–3 images between 20:00. and 22:00). In addition to LST, the dataset also included information on cloud cover and NDVI, the latter used, as explained above, to estimate LAI.

Data processing was performed using the Sentinel Application Platform (SNAP, version 9.0.0), developed by ESA Earth Online (https://earth.esa.int/eogateway/tools/snap, accessed September 15, 2024). A rigorous quality control procedure was implemented to minimize cloud-related interference in Land Surface Temperature (LST) retrievals. Images with more than 10 % cloud cover were excluded, while those with minor cloud contamination were masked using a 3-km buffer around cloud-affected pixels to eliminate potential shading effects on LST.

To enhance data reliability, SUHII values outside the 10th and 90th percentiles were removed, reducing the influence of outliers on mean-based analyses. Following this filtering process, the final dataset consisted of 264 images for Lecce, 168 for Bari, 213 for Turin, and 212 for Milan.

The analysis was conducted over two spatial domains. The first was restricted to the urban extent of each city, where morphological parameters were extracted, while the second covered a broader area encompassing both urban and adjacent rural zones, allowing for more robust statistical comparisons across land use types. Rural areas were defined using land cover classification, selecting regions where the PSF exceeded 95 %.

### 2.4. Statistical analysis

A statistical framework was applied to the database to explore the relationship between the independent variables (urban characteristics) and the dependent variable (SUHII). To reduce redundancy and ensure a parsimonious set of predictors, multicollinearity among the independent variables was assessed through Variance Inflation Factor (VIF) analysis (Salmerón et al., 2018). The reliability of the multiple regression model was evaluated using residual diagnostics (Liu and Liu, 2022).

Model performance was quantified through several statistical metrics, including the root mean square error (RMSE), coefficient of determination ($R^2$), F-statistic and *p*-value. F-statistic indicates whether the regression model provides a better fit to the data than a model that does not contain independent variables. In essence, it checks whether the regression model is useful. If p-value $<0.05$, there is sufficient evidence to conclude that the regression model fits the data better than the model without predictor variables. This result is positive because it means that the predictor variables in the model improve the fit of the model. In general, if none of the predictor variables in the model are statistically significant, the overall F-statistic is also not statistically significant (Sureiman and Mangera, 2020).

To uncover latent structures within the dataset, a multidimensional scaling (MDS) analysis was conducted. The contribution of each independent variable to the observed groupings was further assessed using Similarity Percentage (SIMPER) analysis (Mead, 1992; Davison et al., 2000). This method quantifies the relative influence of each variable on inter-group dissimilarities, identifying those most responsible for variation (Bakker, 2024). By decomposing differences between groups, SIMPER helps isolate key drivers of observed patterns, thereby enhancing interpretation of complex multivariate data. While traditionally employed in ecological studies to determine the dominant factors differentiating biological communities (e.g., Pierri et al., 2010; Rallis et al., 2022), its application in urban micrometeorology offers an innovative perspective.

## 3. Results and discussion

This section presents a preliminary overview of the spatial variability of SUHII in the four cities, in daytime and nighttime conditions. SUHII values correspond to mean values calculated over the JJA periods. This is followed by more detailed statistical analyses aimed at developing the general relationships identified through the statistical model.

### 3.1. Analysis of SUHI

Figure 2 shows the spatial variability of SUHII under daytime conditions, revealing marked differences in both magnitude and spatial extent among the four cities. While Lecce and Milan have already been analysed previously with published results (Esposito et al., 2024), this study extends the analysis to include Turin and Bari, cities selected for their comparable climatic conditions and urban morphologies, to provide a more comprehensive comparison. Lecce and Bari (Fig. 2a and b) exhibit predominantly negative SUHII values across much of their central, densely built-up areas, with intensities typically ranging from −3 °C to −4 °C.This pattern is characteristic of arid and semi-arid environments, as observed in previous case studies such as Doha (Qatar) (Rajeswari et al., 2024) and Erbil (Iraq) (Rasul et al., 2015), where negative SUHII was mainly attributed to changes in soil moisture levels. A similar phenomenon was documented by Donateo et al. (2023), who conducted a detailed analysis of the city of Lecce. Their results confirm the negative SUHII values observed in this study, as they highlighted the presence of a negative air urban heat island in the city center during the early hours of summer days. Albini et al. (2025), show a negative SUHI for Bari, with an average of −2.1 °C calculated over a longer period (i.e., 2013 to 2023). In contrast, Milan and Turin (Fig. 2c and d) show a different heat profile, with positive and substantially higher SUHII values concentrated in central urban areas and industrial zones between 7 and 10 °C, reflecting typical urban heat accumulation patterns found in temperate European cities. These results are in line with the findings of Anniballe et al. (2014) where the daytime SUHI in Milan was estimated to be around 9–10 °C in summer months, as well as those reported in Albini et al. (2025), which show a daytime SUHII of 6.9 °C for Milan and 8.1 °C in Turin for summer months.

Given these marked differences in the magnitude of SUHII across the four cities, a uniform colour scale would not be appropriate, as it would compress or exaggerate spatial variations within individual urban areas. For this reason, each panel in Fig. 2 has been mapped using a locally optimized colour range to more accurately represent the specific internal thermal gradients of each city.

In Fig. 3, all four cities show positive SUHII values during the nighttime hours, reflecting a net accumulation and retention of heat in urban areas after sunset.

Lecce (Fig. 3a) exhibits moderate nocturnal SUHII, predominantly localized in the central urban area, with pick values around

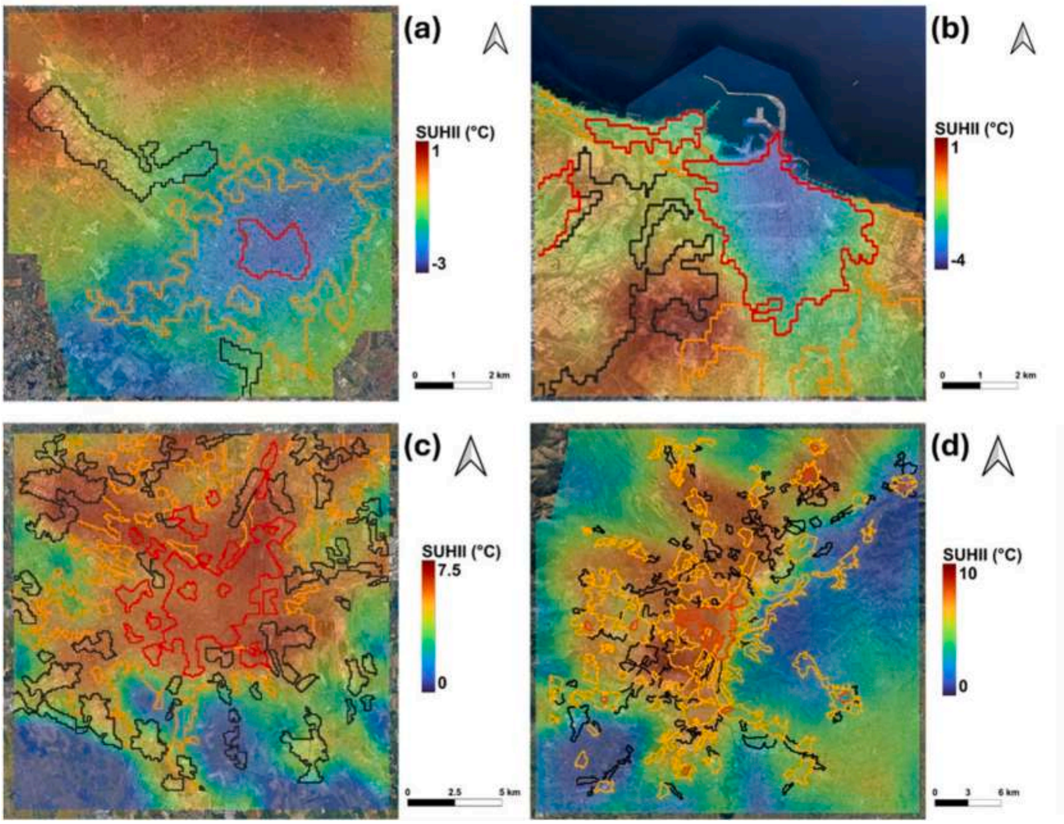


**Fig. 2.** Spatial variability of daytime SUHII across the four analysed cities: Lecce (a), Bari (b), Milan (c), and Turin (d). The SUHII values represent mean conditions during the JJA period. Contour lines indicate the three main CLC classes (CLC 1, 2, 3). Colour scales are not standardized across cities, as SUHII magnitudes differ substantially; this approach enhances the visibility of internal spatial gradients within each urban area.

2.5 °C. Conversely, Bari, Milan, and Turin (Fig. 3b–d) display more intense and spatially extensive patterns, exceeding 4.5 °C in city cores. These findings align with Milelli et al., 2023 and Anniballe et al., 2014, who reported nocturnal SUHII of 4–5 °C in Turin and Milan during summer. The stronger intensity likely reflects greater heat retention in densely built and industrialized zones, driven by variations in land cover, urban form, and the thermal inertia of construction materials.

### 3.2. Statistical analysis

A comprehensive statistical framework was implemented to quantify the influence of urban morphological and surface characteristics on SUHII (Fig. 4). The analysis followed a multi-step approach to ensure both robustness and interpretability of the results. First, multicollinearity among the independent variables was assessed using VIF to remove the most collinear predictors. Next, an MLR was applied to quantify the relative contribution of the selected variables to SUHII variability. The performance and reliability of the model were assessed using diagnostic statistics, including RMSE, $R^2$, F-statistic, and *p*-values.

To complement the regression analysis and explore potential multidimensional relationships between variables, an MDS was conducted. This allowed us to visualize the similarities and differences between cities based on their urban characteristics and SUHII profiles. The contribution of each independent variable to these models was further examined using SIMPER analysis, which allowed us to identify the most influential parameters responsible for the observed spatial differences.

This integrated approach provides both a quantitative estimate of the importance of predictors (via MLR) and a qualitative understanding of their multivariate relationships (via MDS and SIMPER).

To clarify the influence of morphological parameters on SUHII, a detailed analysis was then performed to assess the relationships between the independent variables (urban characteristics) and the dependent variable (SUHII), based on the framework described in section 2.4.

#### 3.2.1. VIF and multiple linear regression analysis

VIF analysis is used to detect and quantify multicollinearity among the independent variables in a multiple linear regression model. Multicollinearity occurs when one or more independent variables are strongly correlated, which can bias coefficient estimates and reduce the clarity and reliability of model interpretation. Table 1 shows the VIF values for all four cities. In all four cases, AR and SVF show high VIF values, suggesting strong multicollinearity with other predictors. Their exclusion was necessary to improve model reliability and interpretability. A VIF threshold of 12.50 was then applied to the remaining variables to reduce collinearity while

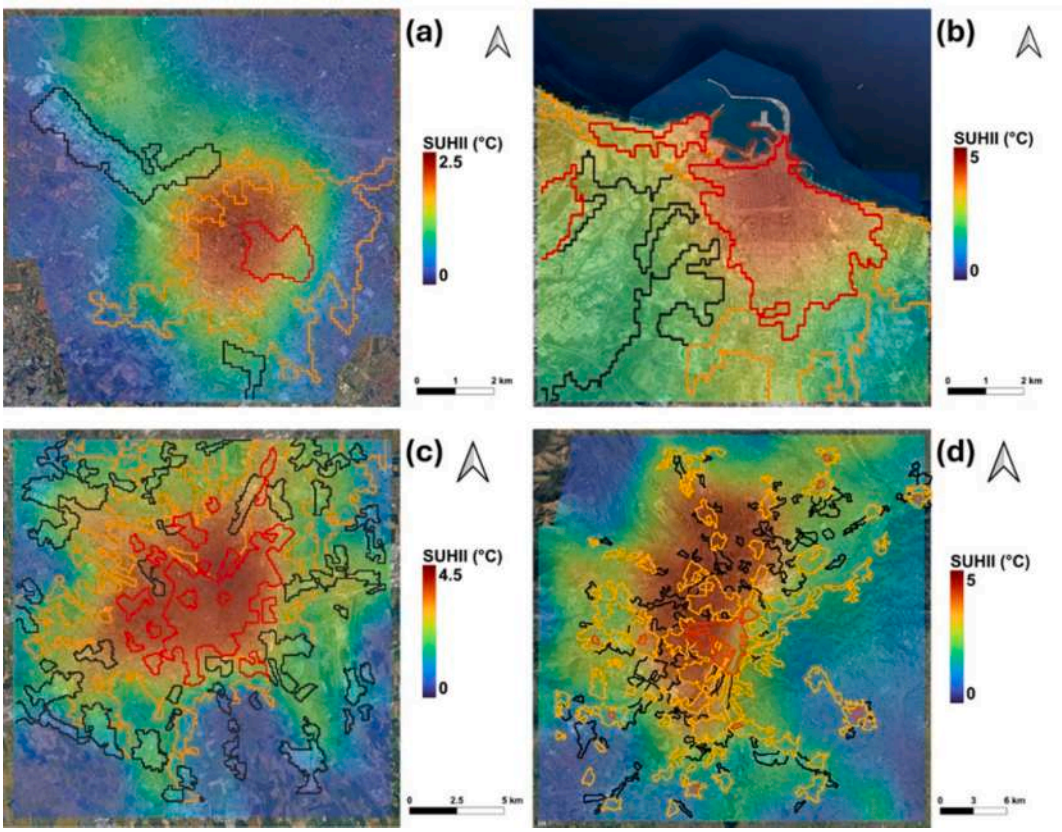


**Fig. 3.** As in Fig. 2 but during nighttime.

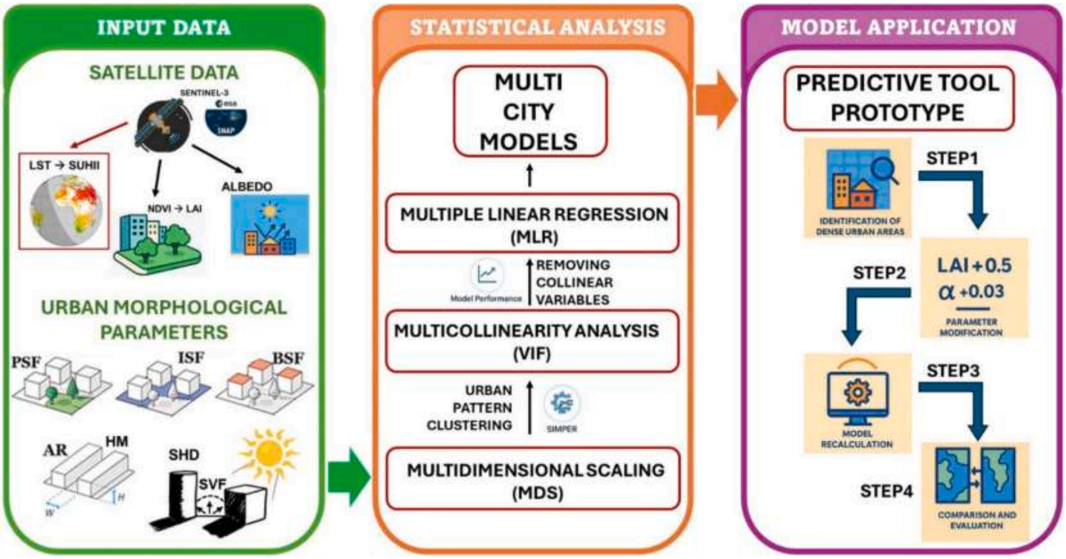


**Fig. 4.** Workflow diagram of the methodological process.

preserving explanatory power. This threshold, slightly higher than conventional values of 5 or 10, was adopted following the recommendations of O'Brien (2007) and Jeng (2023), who highlighted that such limits are empirical rather than absolute and should be adapted to the specific modelling context. The choice of 12.50 ensured the inclusion of the impervious surface fraction (ISF), a key predictor in urban climate studies that consistently exerts a strong influence on land surface temperature (Yuan and Bauer, 2007; Zhang et al., 2022a, 2022b). This additional filtering led to the exclusion of BSF for Lecce, Bari, and Milan, and SHD for Bari, Milan, and Turin. Following standard multicollinearity diagnostics, pairwise correlations among the remaining predictors were examined using the Pearson coefficient, adopting the conventional threshold of $|r| < 0.8$ to identify potential collinearity issues (Kutner et al., 2004). All variable pairs exhibited $|r| < 0.8$, confirming that multicollinearity was effectively mitigated through the VIF filtering and that the retained predictors can be considered statistically independent for regression analysis.

Following the removal of highly collinear variables, multiple linear regression analyses were performed separately for daytime and nighttime scenarios in each city. The logic behind this distinction consists in the Sentinel-3 acquisition schedule which, as described in Section 2.3, collects observations at different local overflight times for day (approximately between 08:00 and 10:00) and night (approximately between 20:00 and 22:00). These analyses reveal both consistent patterns and city-specific variations in the role of urban morphological parameters in modulating the SUHII. Tables 2 (daytime) and 3 (nighttime) present the estimated coefficients (EC) and *p*-values of the multiple linear regression analyses between cities, illustrating how urban morphological parameters influence the SUHI intensity. (See Table 3.)

In Lecce, daytime SUHII shows significant negative associations with ISF, HM, and LAI. This pattern likely results from the tendency for negative daytime SUHI, driven by low moisture in soil and vegetation within the surrounding rural areas. In contrast, SHD and α are not statistically significant during the day, suggesting a limited role. At night, Lecce shows a different pattern: ISF and SHD are positively associated with SUHI. This suggests that areas with significant shadow are also characterized by dense urban built-up, which limits nighttime radiative cooling by trapping longwave radiation within street canyons.

In Bari, daytime results show negative associations between SUHII and ISF and LAI, following the results obtained for Lecce. However, HM and α do not significantly influence daytime temperatures. During the night, Bari reveals significant positive associations between SUHI and ISF and HM, indicating heat retention due to build surfaces and structures, while α shows a strong negative effect, confirming its role in improving nighttime cooling. LAI, however, is not significant.

In Milan, LAI and α are significant during the day, both negatively associated with SUHII, highlighting the cooling benefits of

**Table 1**
VIF values for the four cities, with indication (bold and italics) of values greater than 12.50 (threshold).

| | LECCE | BARI | MILAN | TURIN |
|---|---|---|---|---|
| ISF | 9.92 | 12.16 | 10.53 | 10.04 |
| BSF | ***15.24*** | ***26.82*** | ***15.28*** | 7.81 |
| AR | ***397.48*** | ***139.86*** | ***329.57*** | ***241.99*** |
| SVF | ***345.74*** | ***148.85*** | ***325.33*** | ***181.87*** |
| HM | 2.72 | 3.51 | 3.35 | 2.54 |
| SHD | 1.28 | ***24.78*** | ***15.93*** | ***14.11*** |
| LAI | 2.07 | 4.18 | 6.08 | 4.33 |
| α | 1.83 | 1.75 | 3.2 | 2.12 |

**Table 2**
Results of multiple linear regression in daytime. The *p*-values bolded and underlined are the most significant ones (p-value<0.05). Non-reported variables were not statistically significant.

| | LECCE | | BARI | | MILAN | | TURIN | |
|---|---|---|---|---|---|---|---|---|
| | EC | p-value | EC | p-value | EC | p-value | EC | p-value |
| ISF | −2.50 | ***3.57 × 10^−9*** | −3.55 | ***4.03 × 10^−5*** | −0.26 | 0.18 | 1.15 | ***0.01*** |
| BSF | – | – | – | – | – | – | 0.81 | 0.42 |
| HM | −0.09 | ***6.40 × 10^−4*** | −0.04 | 0.19 | $-3 \times 10^{-3}$ | 0.72 | $-8 \times 10^{-3}$ | 0.65 |
| SHD | 0.01 | 0.36 | – | – | – | – | – | – |
| LAI | −8.19 | ***6.24 × 10^−21*** | −3.10 | ***0.03*** | −5.56 | ***1 × 10^−3*** | −5.09 | ***1 × 10^−3*** |
| α | −12.60 | 0.06 | 12.76 | 0.09 | 7.32 | ***3.75 × 10^−4*** | 15.99 | ***1.06 × 10^−8*** |

**Table 3**
Results of multiple linear regression in nighttime. The p-values bolded and underlined are the most significant ones (p-value<0.05). Non-reported variables were not statistically significant.

| | LECCE | | BARI | | MILAN | | TURIN | |
|---|---|---|---|---|---|---|---|---|
| | EC | p-value | EC | p-value | EC | p-value | EC | p-value |
| ISF | 2.14 | ***3.25 × 10^−14*** | 1.67 | ***1.26 × 10^−5*** | 1.26 | ***1.73 × 10^−12*** | 1.31 | ***5.04 × 10^−7*** |
| BSF | – | – | – | – | – | – | −0.63 | 0.27 |
| HM | $-2 \times 10^{-3}$ | 0.88 | 0.06 | ***1.70 × 10^−4*** | 0.05 | ***3.13 × 10^−13*** | 0.03 | ***5 × 10^−4*** |
| SHD | $1 \times 10^{-3}$ | ***0.01*** | – | – | – | – | – | – |
| LAI | 0.61 | 0.15 | −0.63 | 0.31 | −0.42 | ***1 × 10^−3*** | −1.14 | ***2.59 × 10^−12*** |
| α | −0.58 | 0.89 | −16.53 | ***5.11 × 10^−6*** | −21.47 | ***3.35 × 10^−28*** | −21.44 | ***5.48 × 10^−34*** |

vegetation and reflective surfaces in a complex urban context, while ISF and HM show no significant effects. At night, all variables in Milan are statistically significant: ISF and HM are positively associated with the increase in SUHII, while LAI and α maintain negative associations.

In Turin, the daytime analysis shows that ISF, LAI, and α are significant, with LAI and α negatively correlated with SUHII, while ISF shows an unexpected positive association, probably reflecting localized complexities or spatial interactions. HM and BSF do not significantly influence daytime SUHI. At night, ISF and HM continue to show positive associations with SUHII, in line with heat retention effects, while LAI and α remain negatively associated, reaffirming their cooling role. Again, BSF is not statistically significant at night, indicating its limited role in influencing SUHI intensity at night.

Across the four cities, the impact of urban morphological parameters on SUHII differs markedly between day and night, reflecting local climatic and structural features. During the day, vegetation (LAI) and albedo often show significant negative associations with SUHII especially in Milan and Turin, indicating cooling effects from evapotranspiration and surface reflectivity. At night, ISF consistently correlates with higher SUHII in all cities, highlighting its role in heat retention. HM also becomes more influential at night in Bari, Milan, and Turin, likely due to reduced sky exposure and increased thermal mass limiting radiative cooling.

Overall, ISF and LAI consistently emerge as the most significant variables across all cities and time periods, confirming their key role in shaping urban thermal environments. α, though often significant, shows inconsistent effects, especially during the day, likely due to interactions with surface materials and SHD. HM appears to play a dual role: it may reduce heat through shading in the morning, while in the evening it likely contributes to heat retention.

Several studies have used multiple linear regression (MLR) models to investigate the determinants of urban heat island (UHI) intensity and surface temperature variability (e.g., Garzón et al., 2021; Deng et al., 2021; Oukawa et al., 2022). While these works have demonstrated the potential of regression-based approaches to quantify the influence of vegetation and imperviousness on land surface temperature (LST), they are often limited to single-city analyses, rely on a narrow set of spectral indices (e.g., NDVI, NDBI), and lack cross-comparative consistency across climatic and morphological contexts.

The present study advances this body of research by integrating morphological, radiative, and biophysical parameters derived from high-resolution, geometry-based datasets. Predictors such as building height, surface fraction, albedo, and LAI ensure a physically consistent representation of the three-dimensional urban fabric, improving the explanatory power of the model and enabling meaningful comparisons between cities with different climatic and structural characteristics. Moreover, by combining MLR with multivariate techniques such as MDS and SIMPER, the proposed framework explicitly links high-resolution urban form descriptors with satellite-derived thermal patterns. This integrated approach bridges the gap between statistical and physically based analyses, providing a reproducible and transferable tool for assessing the drivers of surface urban heat and supporting climate-adaptive urban planning.

### *3.2.2. Residual analysis and city-specific regression equations*

To assess the validity and reliability of the multiple linear regression models, residual diagnostics were performed to verify key assumptions, including normality and homoscedasticity. The results are illustrated in Figs. 5 and 6, which show both quantile-quantile (Q-Q) plots and histograms comparing the empirical residual distributions with the theoretical quantiles of a standard normal distribution. The Q-Q plots provide a visual assessment of normality, while the histograms offer a complementary view of the residual density. When the residuals align closely with the 1:1 reference line and exhibit a symmetric Gaussian shape, the model can be included as statistically robust. Deviations in the tails of the distribution are common in empirical datasets and do not compromise the validity of the model, as they often reflect natural variability or rare observations rather than structural bias (Gelman and Hill, 2006; Barker and Shaw, 2015).

Under daytime conditions (Fig. 5), the residuals show varying degrees of conformity to normality in the four cities. Lecce and Milan (Fig. 5a,b and Fig. 5e,f) show strong alignment with the theoretical quantiles and nearly symmetrical residual distributions centered around zero, confirming the robustness of the models. Bari (Fig. 5c,d) has a bimodal distribution and larger deviations in the tails, indicating possible heteroscedasticity or unmodeled variability. Turin (Fig. 5g,h), although generally aligned, shows slightly heavier tails and dispersion in the upper quantiles, suggesting localized anomalies or space-dependent effects.

During the nighttime period (Fig. 6), the alignment of residuals with normality improves in all cities. Lecce and Bari (Fig. 6a,b and Fig. 6c,d) show compact and symmetric residual distributions centered near zero, indicating that the model assumptions are well satisfied. Milan (Fig. 6e,f) maintains good adherence, with modest right-skewness linked to minor heteroscedastic behaviour. Turin (Fig. 6g,h) once again shows heavier tails and moderate asymmetry, indicating localized deviations from normality possibly related to intra-urban heterogeneity.

Residual diagnostics indicate that the multiple linear regression models are broadly consistent with the normality assumption in the four cities, albeit with varying degrees of deviation from the ideal distribution. The deviations observed in Bari and, to a minor extent, in Turin suggest the presence of potential unmodeled factors, such as local-scale variability, nonlinear associations, or interaction effects. Although these deviations do not compromise the overall validity of the models, they highlight opportunities for refinement and suggest that the integration of more advanced approaches (e.g., mixed-effects models or nonlinear terms) could further improve model performance in future analyses. A comparative summary of the residual diagnostics is reported in Table 4, which outlines the main characteristics and implications for model performance.

Residual assumptions were also evaluated using formal statistical tests, including the Kolmogorov-Smirnov test for normality (Massey, 1951), the Breusch-Pagan test for homoscedasticity (Breusch and Pagan, 1979), and the Durbin-Watson statistic for independence (Durbin and Watson, 1950). These tests complement graphical diagnostics by providing quantitative evidence on the validity of the model.

As summarized in Table 5, all models satisfy the normality assumption of the residuals ($p > 0.05$), confirming the suitability of the linear specification. Homoscedasticity is generally respected in all cities and periods, except for Lecce (nighttime), which shows a slight but significant heteroscedasticity ($p = 0.003$). The Durbin-Watson statistic indicates the independence of the residuals for most daytime models (DW $\approx$ 1.5–2.0), while slightly lower values are observed in nighttime conditions, particularly in Milan and Turin, suggesting positive autocorrelation related to spatial dependencies in surface temperature models.

Overall, these results confirm the robustness of the regression models: the main assumptions are satisfied and the small deviations identified are consistent with the spatially continuous nature of the land surface temperature patterns and do not compromise the reliability of the inferred relationships.

Based on the results of the multiple linear regression analyses, city-specific regression equations were derived for each case study, as summarized in Table 6a, and in Table 6b are presented the standard error (SE) and the confidence interval (CI) for each independent

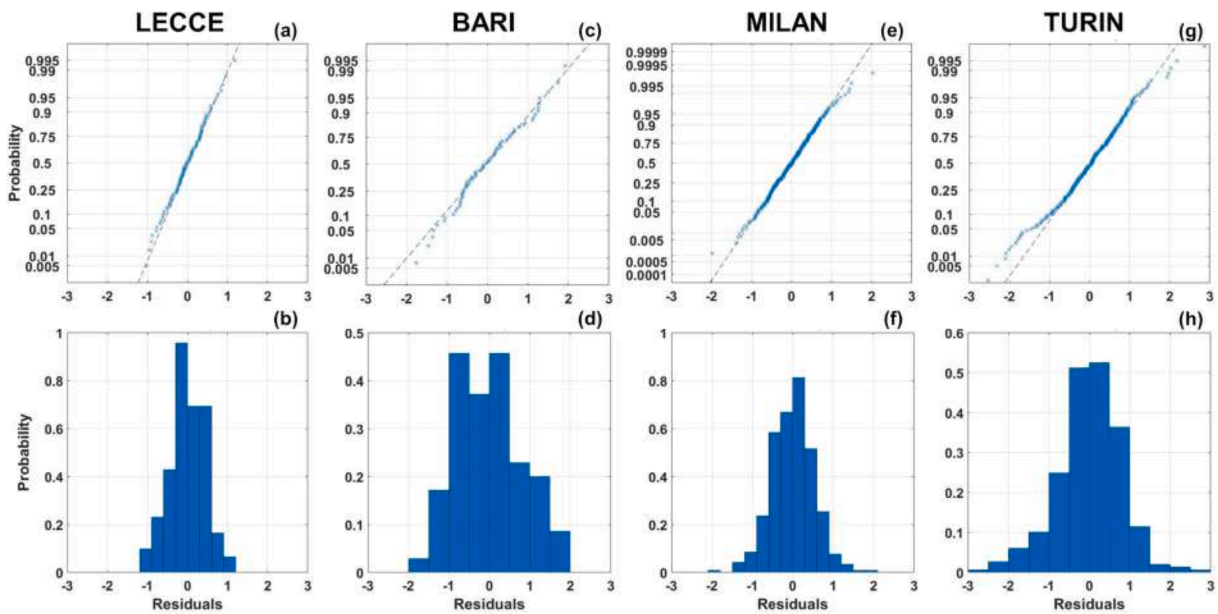


**Fig. 5.** Q-Q plot (top) and histogram (bottom) of the residuals for Lecce (a and b), Bari (c and d), Milan (e and f) and Turin (g and h) in daytime.

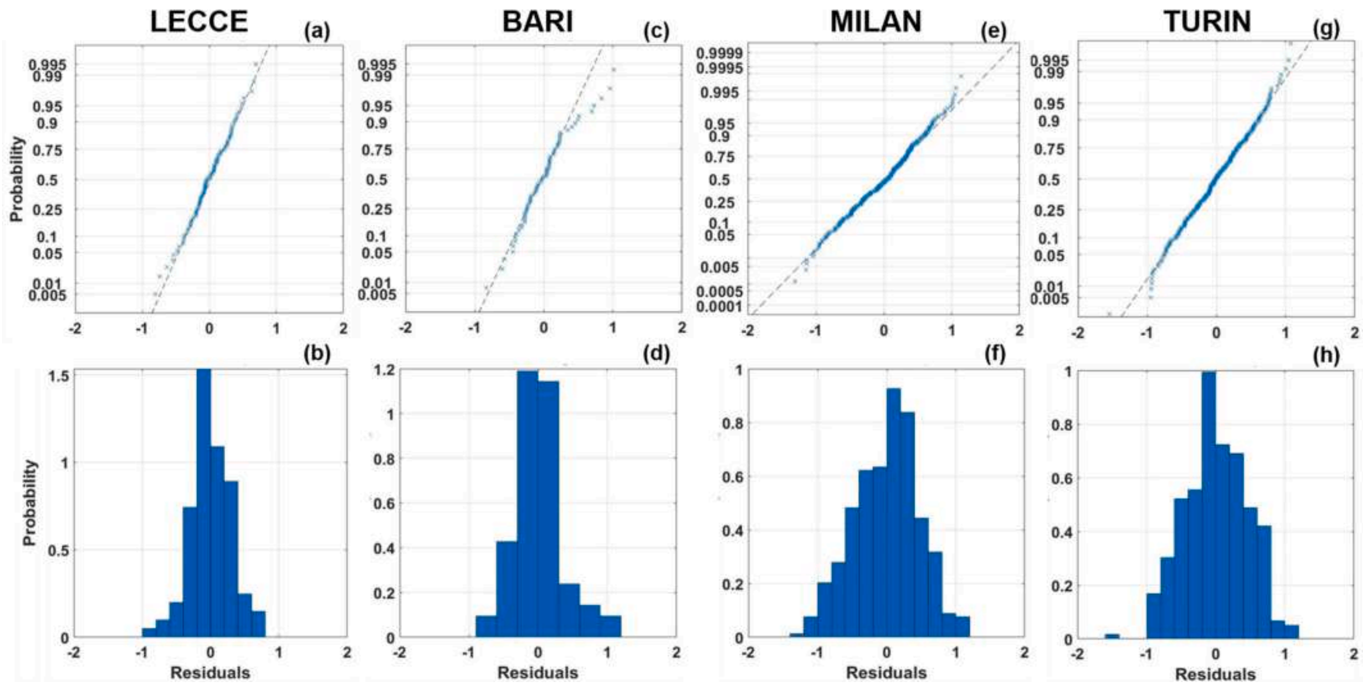


**Fig. 6.** As in Fig. 5 but in nighttime.

**Table 4**
Summary of residual diagnostics for the four analysed cities.

| City | Main residual features | Normality conformity | Diagnostic interpretation |
|---|---|---|---|
| Lecce | Slight tail deviations, near-symmetric histogram | High | Model residuals largely satisfy normality; minor outliers reflect natural variability. |
| Bari | Bimodal distribution, pronounced tails | Moderate | Possible heteroscedasticity or unmodeled variability; residuals indicate local-scale effects. |
| Milan | Slight positive skew, symmetric core distribution | Good | Minor heteroscedastic behaviour; model remains statistically robust. |
| Turin | Heavier tails, moderate skewness | Moderate | Localized deviations likely linked to intra-urban heterogeneity or spatial clustering. |

**Table 5**
Diagnostic tests of regression assumptions for daytime and nighttime models.

| City | Time | Kolmogorov–Smirnov | Breusch–Pagan | Durbin–Watson | Interpretation |
|---|---|---|---|---|---|
| Lecce | Day | D = 0.03, $p$ = 1.51 Normal | LM = 0.65, $p$ = 0.42 Homoscedastic | DW = 1.53 Independent | All assumptions satisfied |
| | Night | D = 0.07, $p$ = 0.64 Normal | LM = 8.62, p = 0.003 Heteroscedastic | DW = 1.17 Positive autocorr. | Minor issues in variance & independence |
| Bari | Day | D = 0.07, p = 0.95 Normal | LM = 0.004, $p$ = 0.95 Homoscedastic | DW = 1.54 Independent | All assumptions satisfied |
| | Night | D = 0.10, $p$ = 0.35 Normal | LM = 0.28, $p$ = 0.60 Homoscedastic | DW = 1.28 Slight autocorr. | Generally robust |
| Milan | Day | D = 0.02, $p$ = 1.03 Normal | LM = 3.81, $p$ = 0.05 Near homosced | DW = 0.76 Positive autocorr. | Spatial dependency suspected |
| | Night | D = 0.05, $p$ = 0.24 Normal | LM = 0.16, $p$ = 0.69 Homoscedastic | DW = 0.85 Positive autocorr. | Residuals correlated |
| Turin | Day | D = 0.04, $p$ = 0.56 Normal | LM = 3.08, $p$ = 0.08 Near homosced. | DW = 0.92 Positive autocorr. | Slight correlation |
| | Night | D = 0.02, $p$ = 1.38 Normal | LM = 2.65, $p$ = 0.10 Homoscedastic | DW = 1.10 Slight autocorr. | Acceptable |

variables for each model. It is worth noting that predictors with $p$-values greater than 0.05 were retained in the final regression models. Their exclusion produced negligible changes in the $R^2$ (less than 0.01) and did not significantly affect the interpretation of the model. Consequently, these predictors were retained to preserve the consistency of the model across different cities.

### *3.2.3. Model performance and statistical evaluation*

To assess the performance of the city-specific multiple linear regression model, performance indicators (RMSE and $R^2$) and statistical tests (F-test and p-value) were calculated, as described in subsection 2.4. These indicators provide a concise assessment of model fit and statistical significance. The results are summarized in Table 7, where daytime results are presented at the top and nighttime results at the bottom.

During daytime conditions, the model demonstrates strong predictive performance in Lecce, characterized by low error and robust statistical indicators, whereas Bari exhibits limited reliability, with higher error values and insufficient model adequacy. Milan yields the most accurate and consistent daytime results, followed by Turin, which also shows satisfactory model performance. Under nighttime conditions, all cities experience a notable enhancement in model accuracy and statistical reliability, with RMSE values consistently below 0.47 °C. While Lecce exhibits only marginal improvement, Bari shows a substantial reduction in error, indicating a more stable and predictable nocturnal thermal response. This could be due to the predominant effect of breeze regimes, which can significantly determine temperature trends in urban environments during daylight hours.

Milan and Turin exhibit stable and consistent model performance across both diurnal periods, highlighting the impact of daily thermal dynamics on urban temperature modelling. The reduced variability during nighttime facilitates improved predictive accuracy, especially in cities where daytime model performance is comparatively weaker. All models exhibit highly significant p-values, confirming the statistical robustness of the selected predictors.

Overall, the results indicate that Milan and Turin consistently exhibit high model accuracy, while Lecce and Bari perform better during nighttime, reflecting distinct urban dynamics and diurnal responses. The greater consistency observed in nighttime models can be attributed to a more stable energy balance between the surface and atmosphere, as the absence of direct solar radiation reduces local thermal variability, shading effects and anthropogenic heating. In coastal cities such as Bari, daytime surface temperature variability is further modulated by sea breezes. At night, the thermal regime is mainly governed by the uniform release of heat accumulated during the day, leading to a more thermodynamically stable and radiatively controlled urban boundary layer, which strengthens the statistical relationship between land surface characteristics and observed LST patterns.

### *3.2.4. Urban pattern clustering*

To develop a general multiple linear regression model applicable across cities (hereinafter referred to as the "multi-city equation"),

**Table 6**
Summary of the city-specific multiple linear regression equations and corresponding statistical indicators.

a. City-specific regression equations from multiple linear regression analyses

| | |
|---|---|
| **DAY** | |
| LECCE | $y = 11.51–2.48 \times ISF - 0.08 \times HM + 9.4 \times 10^{-4} \times SHD - 8.19 \times LAI - 12.60 \times \alpha$ |
| BARI | $y = 1.49–3.55 \times ISF - 0.04 \times HM - 3.10 \times LAI + 12.76 \times \alpha$ |
| MILAN | $y = 11.42–0.26 \times ISF - 0.003 \times HM - 5.56 \times LAI + 7.32 \times \alpha$ |
| TURIN | $y = 8.96 + 1.15 \times ISF + 0.81 \times BSF + 0.008 \times HM - 5.09 \times LAI + 15.99 \times \alpha$ |
| **NIGHT** | |
| LECCE | $y = -0.59 + 2.14 \times ISF - 0.002 \times HM + 0.001 \times SHD + 0.61 \times LAI - 0.58 \times \alpha$ |
| BARI | $y = 5.19 + 1.67 \times ISF + 0.06 \times HM - 0.63 \times LAI - 16.53 \times \alpha$ |
| MILAN | $y = 5.02 + 1.26 \times ISF + 0.06 \times HM - 0.42 \times LAI - 21.47 \times \alpha$ |
| TURIN | $y = 7.00 + 1.31 \times ISF - 0.63 \times BSF + 0.04 \times HM - 1.14 \times LAI - 21.44 \times \alpha$ |

b. Standard error (SE) and confidence interval (CI) for each independent variables for each models in daytime and nighttime cases.

| | ISF | | | BSF | | | HM | | | SHADING | | | LAI | | | α | | |
|---|---|---|---|---|---|---|---|---|---|---|---|---|---|---|---|---|---|---|
| | SE | CI | | SE | CI | | SE | CI | | SE | CI | | SE | CI | | SE | CI | |
| **DAY** | | | | | | | | | | | | | | | | | | |
| LECCE | 0.38 | −3.23 | −1.73 | – | – | – | 0.02 | −0.13 | −0.03 | $1 \times 10^{-3}$ | $-1 \times 10^{-3}$ | $3 \times 10^{-3}$ | 0.67 | −9.51 | −6.86 | 6.61 | −25.56 | 0.35 |
| BARI | 0.80 | −5.14 | −1.97 | – | – | – | 0.03 | −0.11 | 0.02 | – | – | – | 1.42 | −5.89 | −0.31 | 7.56 | −2.06 | 27.60 |
| MILAN | 0.19 | −0.65 | 0.12 | – | – | – | $8 \times 10^{-3}$ | −0.02 | 0.01 | – | – | – | 0.14 | −5.85 | −5.26 | 2.03 | 3.32 | 11.31 |
| TURIN | 0.45 | 0.27 | 2.04 | 1.00 | −1.16 | 2.80 | 0.02 | −0.03 | 0.04 | – | – | – | 0.27 | −5.63 | −4.55 | 2.71 | 10.67 | 21.32 |
| **NIGHT** | | | | | | | | | | | | | | | | | | |
| LECCE | 0.24 | 1.67 | 2.61 | – | – | – | 0.02 | −0.03 | 0.03 | $6 \times 10^{-4}$ | $4 \times 10^{-4}$ | $3 \times 10^{-3}$ | 0.42 | −0.22 | 1.45 | 4.15 | −8.72 | 7.56 |
| BARI | 0.35 | 0.98 | 2.37 | – | – | – | 0.01 | 0.03 | 0.09 | – | – | – | 0.62 | −1.86 | 0.59 | 3.32 | −23.04 | −10.01 |
| MILAN | 0.17 | 0.93 | 1.6 | – | – | – | $7 \times 10^{-3}$ | 0.04 | 0.07 | – | – | – | 0.13 | −0.67 | −0.16 | 1.80 | −25.00 | −17.95 |
| TURIN | 0.26 | 0.82 | 1.82 | 0.57 | −1.76 | 0.49 | 0.01 | 0.02 | 0.06 | – | – | – | 0.16 | −1.45 | −0.84 | 1.54 | −24.47 | −17.41 |

**Table 7**
Model performance based on statistical metrics. Asterisks indicate the statistical significance of the overall regression model ($p < 0.05$).

| | RMSE (°C) | $R^2$ | F-test | p-value |
|---|---|---|---|---|
| **DAY** | | | | |
| Lecce | 0.47 | 0.74 | 55.30 | $1.24 \times 10^{-26}$* |
| Bari | 0.83 | 0.51 | 17.30 | $1.06 \times 10^{-9}$* |
| Milan | 0.53 | 0.94 | $1.48 \times 10^{3}$ | 0* |
| Turin | 0.80 | 0.86 | 353 | 0* |
| **NIGHT** | | | | |
| Lecce | 0.30 | 0.75 | 58 | $2.25 \times 10^{-27}$* |
| Bari | 0.37 | 0.83 | 80.20 | $2.03 \times 10^{-24}$* |
| Milan | 0.47 | 0.83 | 485 | 0* |
| Turin | 0.46 | 0.86 | 364 | 0* |

the MDS was employed to evaluate the robustness of this approach. Variables AR and SVF were excluded from the MDS analysis due to their consistently high VIF values across all cities, which could introduce multicollinearity-related distortions. The objective of the analysis was to examine inter-city relationships, identify commonalities in urban and environmental characteristics, and assess whether a shared data structure could be reliably captured. The quality of the MDS configuration was quantified using the stress value, while a SIMPER analysis was performed to identify the contribution of individual variables to inter-city dissimilarities. As illustrated in the MDS graph (Fig. 7), distinct and interpretable clustering patterns emerge. Lecce and Bari, located in southern Italy, are positioned at the top of the graph and show a relatively more scattered distribution. This distribution suggests greater internal variability in their urban and environmental characteristics, potentially driven by different morphological structures and local environmental conditions within each city.

In contrast, Milan and Turin exhibit compact and closely aligned clusters near the horizontal axis. Their proximity and overlap involve a high degree of similarity and low internal variability in their urban and environmental characteristics. This consistent pattern supports the hypothesis that a single regression model can effectively represent both cities. These groupings reflect the underlying similarities and differences in their feature spaces, as revealed by MDS analysis, and provide a data-driven basis for developing targeted models. The resulting stress value of 0.21 falls within an acceptable range, indicating a reasonable fit between the reduced two-dimensional configuration and the original high-dimensional data structure (Sturrock and Rocha, 2000).

The percentage contribution of different urban morphological and environmental variables to the studied phenomenon was assessed from the SIMPER analysis. The variables that contribute most to the observed patterns are ISF, albedo, BSF and HM, which show similar levels of contribution, ranging from about 17 % to 18 %. LAI follows closely, reinforcing its importance in influencing the

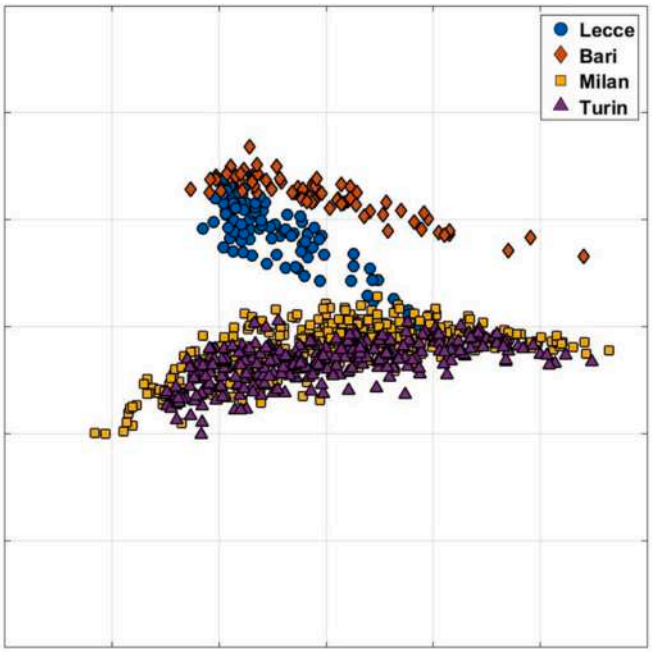


**Fig. 7.** MDS plot showing the spatial relationships between the data points in a reduced two-dimensional space. The points are positioned based on their pairwise dissimilarities, with similar cases grouped together and dissimilar ones separated.

variability of the studied phenomenon. In contrast, shading shows a lower contribution (10 %), highlighting a relatively minor role in shaping the observed spatial patterns. The results indicate that built and surface-related characteristics (such as imperviousness, albedo, and urban morphology) are the primary drivers, while vegetation-related parameters have a comparatively smaller influence.

### 3.3. *Development of multi-city equation*

The distinct spatial separation between the Lecce–Bari cluster and the Milan–Turin cluster in the MDS analysis (Fig. 7) supports the rationale for developing two separate generalized regression models: one for the southern cities (Lecce and Bari) and another for the northern cities (Milan and Turin). The similarity between Milan and Turin suggests a high level of homogeneity in their urban and environmental features. Although Lecce and Bari are less tightly clustered, a common regression equation was also developed for these two cities.

To account for diurnal variability in urban thermal behaviour, separate models were constructed for daytime and nighttime conditions. The same modelling framework used for the city-specific regressions was applied to assess whether a single equation could reliably capture the temperature dynamics of each city pair across different times of day.

#### 3.3.1. *Milan-Turin model*

In the Milan–Turin case, VIF analysis identified AR and SVF as the variables with the highest multicollinearity, with values of 200.26 and 192.61, respectively. All remaining predictors had VIF values below the threshold of 12.50. To enhance model robustness, AR and SVF were excluded from the analysis. Multiple linear regression was then performed using the remaining variables to model temperature dynamics during both daytime and nighttime periods.

During the day, ISF and α are positively correlated, while BSF, SHD and LAI show significant negative effects. HM, on the other hand, does not show a significant influence during the day. The overall model fit is strong, with high descriptive ability and low prediction error, indicating reliable performance.

At night, all variables were statistically significant. ISF continues to have a positive effect, while BSF, SHD, and LAI maintain their negative relationships. α, positively correlated with SUHII during the day, becomes strongly negative at night, reflecting post-sunset energy dynamics and material properties. Its spatial variability is limited, with the highest values found in industrial areas characterized by large, low-rise buildings and reflective roofs. These areas, fully exposed to solar radiation and lacking shading, reach higher daytime LST despite their elevated α. After sunset, their open geometry and low BSF enhance radiative cooling, promoting rapid heat release and pronounced nighttime temperature drops. This behaviour is consistent with the observations of Pappaccogli et al. (2025), where industrial LCZ areas in Milan have the highest LST during the day, followed by rapid cooling in the evening. HM, while not influencing the daytime model, becomes a significant positive factor at night, suggesting that taller buildings may retain heat or influence the urban microclimate more markedly at night. The nighttime model also fits well, capturing most of the variability with relatively low errors (Table 8 and Table 9).

In the daytime model, all included variables except HM exert a statistically significant influence on the dependent variable, confirming strong model performance. In the nighttime case, BSF was excluded due to lack of significance.

Figure 8a–d presents the residual analysis for the Milan–Turin regression models under daytime and nighttime conditions. In the daytime model (Figs. 8a,b), the Q-Q plot indicates that residuals generally follow the theoretical normal distribution, with minor deviations in the right tail. The corresponding histogram supports this pattern, although exhibiting slight concentration of positive residuals. Despite this small skewness, the residuals remain well centered around zero, indicating that the assumptions of normality and homoscedasticity are largely satisfied.

In contrast, the nighttime model (Fig. 8c,d) exhibits stronger statistical performance. The Q-Q plot shows residuals closely aligned with the 45° reference line, with minimal deviations across the distribution. The corresponding histogram confirms a symmetric, narrow distribution centered near zero, with no signs of skewness or heavy tails. Overall, residual diagnostics support the statistical validity of both models.

#### 3.3.2. *Lecce-Bari model*

As in the previous case, VIF analysis was conducted to identify and remove highly collinear variables. In the Lecce–Bari case, BSF,

**Table 8**
Results of multiple linear regression in daytime and nighttime for Milan-Turin model. The *p*-values bold and underlined are the most significant ones (p-value<0.05).

| MILAN-TURIN MODEL | | | | |
|---|---|---|---|---|
| | DAY | | NIGHT | |
| | EC | p-value | EC | p-value |
| ISF | 0.99 | $\mathbf{3 \times 10^{-3}}$ | 0.93 | $\mathbf{1.84 \times 10^{-6}}$ |
| BSF | −3.17 | $\mathbf{1.72 \times 10^{-7}}$ | −1.08 | 0.01 |
| HM | −0.01 | 0.19 | 0.03 | $\mathbf{1.54 \times 10^{-7}}$ |
| SHD | −0.12 | $\mathbf{1.91 \times 10^{-21}}$ | −0.14 | $\mathbf{1 \times 10^{-4}}$ |
| LAI | −5.55 | $\mathbf{1 \times 10^{-4}}$ | −0.84 | $\mathbf{1.27 \times 10^{-16}}$ |
| α | 14.80 | $\mathbf{9.14 \times 10^{-18}}$ | −14.78 | $\mathbf{4.03 \times 10^{-43}}$ |

**Table 9**
Model performance and multi-city equations for Milan-Turin case.

| RMSE (°C) | $R^2$ | F-statistic | p-value |
|---|---|---|---|
| **DAY** | | | |
| $y = 25.90 + 0.99 \times ISF - 3.17 \times BSF - 0.01 \times HM - 0.12 \times SHD - 5.55 \times LAI + 14.80 \times \alpha$ | | | |
| 0.69 | 0.90 | $1.03 \times 10^3$ | $<1 \times 10^{-6}$ |
| **NIGHT** | | | |
| $y = 23.03 + 0.93 \times ISF - 1.08 \times BSF + 0.03 \times HM - 0.14 \times SHD - 0.84 \times LAI - 17.52 \times \alpha$ | | | |
| 0.48 | 0.83 | 571 | $<1 \times 10^{-6}$ |

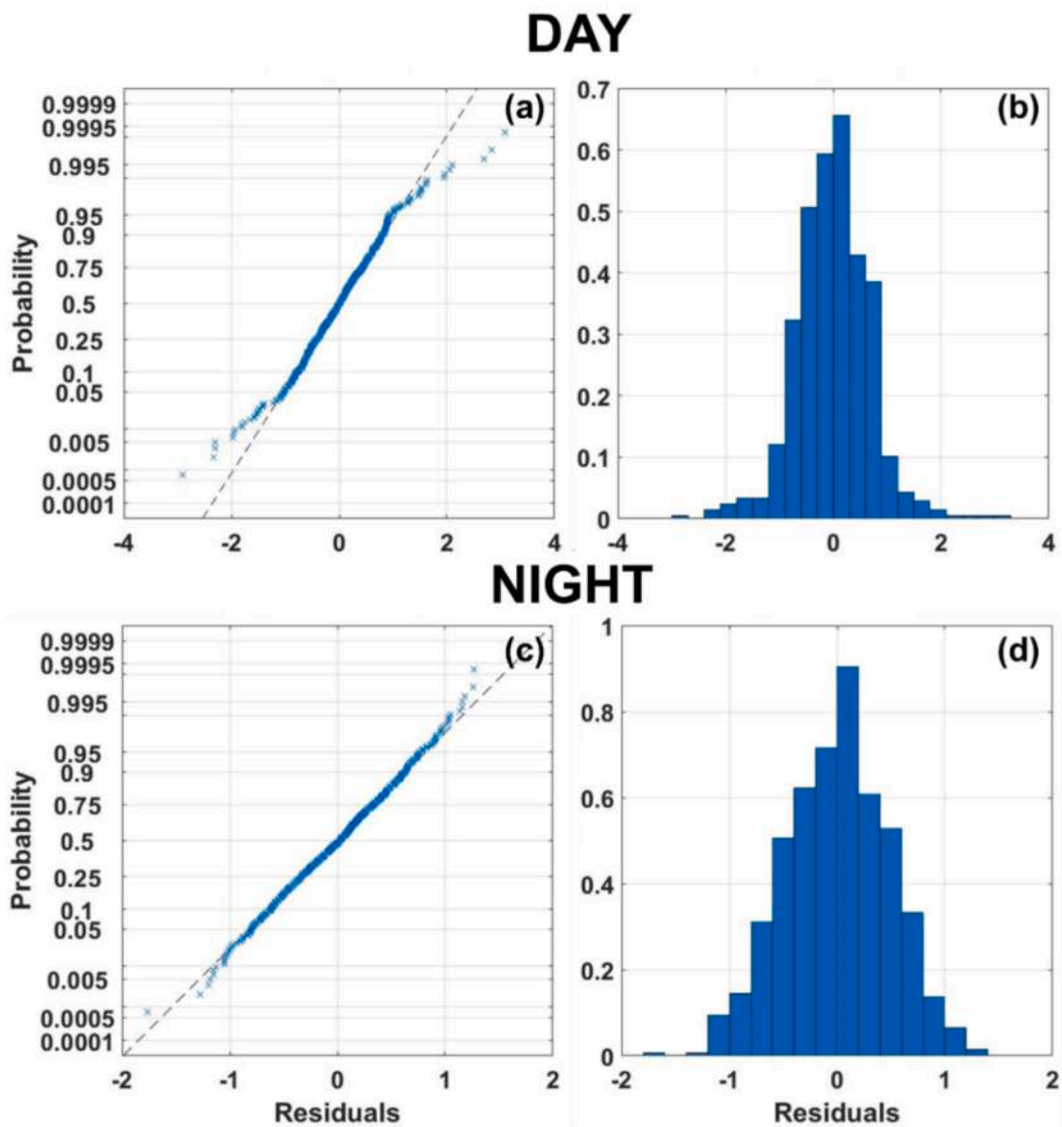


**Fig. 8.** Q-Q plot (left) and histogram (right) of the residuals for Milan-Turin case in daytime (top) e nighttime (bottom).

AR, and SVF exhibited substantial multicollinearity, with VIF values of 15.12, 114.63, and 106.92, respectively, while all other variables remained below the threshold of 12.50. These three variables were excluded from further analysis. Multiple linear regression models were then developed for both daytime and nighttime scenarios using the remaining predictors.

In the daytime case, ISF, HM, and LAI showed significant associations with the dependent variable, whereas the model error is within an acceptable range, supporting a reasonably good fit (Table 11).

At night, the model's performance improves significantly. The same set of predictors was used, but the model captured a much larger share of variance with greater reliability. ISF, SHD, and α are significant nighttime predictors.

These results highlight a shift in the influence of urban form and vegetation between day and night, underscoring the dynamic nature of the factors that determine surface temperature in urban environments (Table 10 and 11).

Specifically, ISF has a consistently strong influence on SUHII both during the day and at night, the effects of the other predictive factors vary depending on the time of day. SHD has a significant influence during nighttime, likely due to reduced solar exposure in the late afternoon and the resulting enhanced radiative cooling during the early evening hours. In contrast, HM and LAI are only significant in the daytime model, suggesting that their influence is likely related to daytime-specific processes, such as solar radiation exposure, heat accumulation in urban structures, and evapotranspiration.

Analysis of the residuals for the Lecce-Bari case in daytime and in nighttime confirms the overall reliability and robustness of the regression models (Fig. 9). During daylight hours, the Q-Q plot (Fig. 9a) shows that the residuals closely follow the 45° reference line, particularly in the central range, suggesting that the normality assumption is largely satisfied. Slight deviations in the tails indicate thin deviations from normality, although they are not substantial enough to undermine the validity of the model. The corresponding histogram (Fig. 9b) reveals an approximately Gaussian distribution centered around zero, with a slight skew to the left due to a longer tail on the negative side.

In the night scenario, the residuals show better fit to the normality hypothesis. The Q-Q plot (Fig. 9c) shows minimal deviation from the baseline for the entire range of values, while the histogram (Fig. 9d) shows a more symmetrical and normally distributed trend, centered on zero, with less skewness than in the daytime case. These features indicate that the errors are well distributed and that the nighttime model is particularly stable.

Overall, both models satisfy the key assumption of a normal distribution of residuals, with the nighttime model showing slightly superior behaviour. These results validate the adequacy of the regression approach for both periods and support the statistical reliability of the results obtained.

### *3.4. Model comparison*

To compare the observed data with model outputs derived from different approaches (city-specific and multi-city models), three SUHII-related maps were produced for each city (Figs. 10–11): SUHII from observed data (OBS), SUHII estimated using city-specific models (MOD1), and SUHII estimated using the multi-city model (MOD2). To support this comparison, mean differences between modelled and observed data (MOD1-OBS and MOD2-OBS, in °C) were also calculated for each city, including the three main Corine Land Cover (CLC) classes (CLC_1, CLC_2 and CLC_3) during daytime and nighttime periods. The three CLC classes were selected considering the 1 km spatial resolution and the size of the chosen cities. Although less detailed than other classifications (e.g., LCZ or Urban Atlas), the CLC provides a statistically robust sample and greater spatial continuity within homogeneous urban areas, reducing the inclusion of small, heterogeneous patches that may exhibit anomalous behaviour. This consistency is particularly important to ensure reliable comparisons across the different models applied. Results in Table 12 highlight important differences in model performance across cities, land cover types, and times of day. Overall, MOD1 (the city-specific model) demonstrates a better fit to observed SUHII values, particularly during the nighttime period. This is most evident in cities like Bari and Milan, where MOD1 maintains low bias across most CLC classes, suggesting that tailoring the model to local conditions leads to more accurate representation of urban thermal behaviour.

During the daytime, both models perform reasonably well, but their accuracy varies by city. In Bari and Milan, MOD1 provides a close match to observations, indicating good daytime fitting across urban classes. In contrast, in Lecce and Turin, MOD1 tends to overestimate SUHII, particularly in more urbanized areas (CLC 1 and CLC 2). MOD2 (the multi-city/generalized model) shows improved agreement with observations during the day, reducing some of the over- and underestimation seen in MOD1. This suggests that MOD2 may generalize better in certain settings where local model calibration is less effective, particularly in southern cities with distinct urban forms or climatic conditions.

At night, MOD2 exhibits significant biases, particularly in Bari, where it consistently underestimates SUHII across all land cover classes. This underperformance suggests that the generalized model struggles to capture localized nocturnal processes, such as heat retention in densely built areas or region-specific meteorological conditions. In Lecce, by contrast, MOD2 even overestimates SUHII in some land cover classes, highlighting inconsistent behaviour across cities. Meanwhile, MOD1 remains relatively stable and generally closer to observations, reinforcing the value of local calibration for accurately modelling nighttime urban heat dynamics.

**Table 10**
As in Table 8 but for Lecce-Bari model.

| LECCE-BARI MODEL | | | | |
|---|---|---|---|---|
| | DAY | | NIGHT | |
| | EC | p-value | EC | p-value |
| ISF | −3.28 | $\boldsymbol{3 \times 10^{-3}}$ | 3.95 | $\boldsymbol{1.41 \times 10^{-23}}$ |
| HM | −0.08 | $\boldsymbol{4 \times 10^{-4}}$ | 0.03 | 0.07 |
| SHADING | $-7 \times 10^{-3}$ | 0.44 | 0.09 | $\boldsymbol{1.24 \times 10^{-26}}$ |
| LAI | −5.41 | $\boldsymbol{1.04 \times 10^{-12}}$ | −0.23 | 0.67 |
| ALBEDO | 6.99 | 0.16 | −25.78 | $\boldsymbol{1.09 \times 10^{-9}}$ |

**Table 11**
As in Table 9 but for Lecce-Bari model.

| RMSE | $R^2$ | F − statistic | p − value |
|---|---|---|---|
| **DAY** | | | |
| $y = 6.20–3.28 \times ISF - 0.08 \times HM - 0.007 \times SHD – 5.41 \times LAI + 6.99 \times \alpha$ | | | |
| 0.70 | 0.55 | 39 | $2.30 \times 10^{-26}$ |
| **NIGHT** | | | |
| $y = -9.22 + 3.95 \times ISF + 0.03 \times HM + 0.09 \times SHD – 0.23 \times LAI – 25.78 \times \alpha$ | | | |
| 0.56 | 0.81 | 139 | $1 \times 10^{-36}$ |

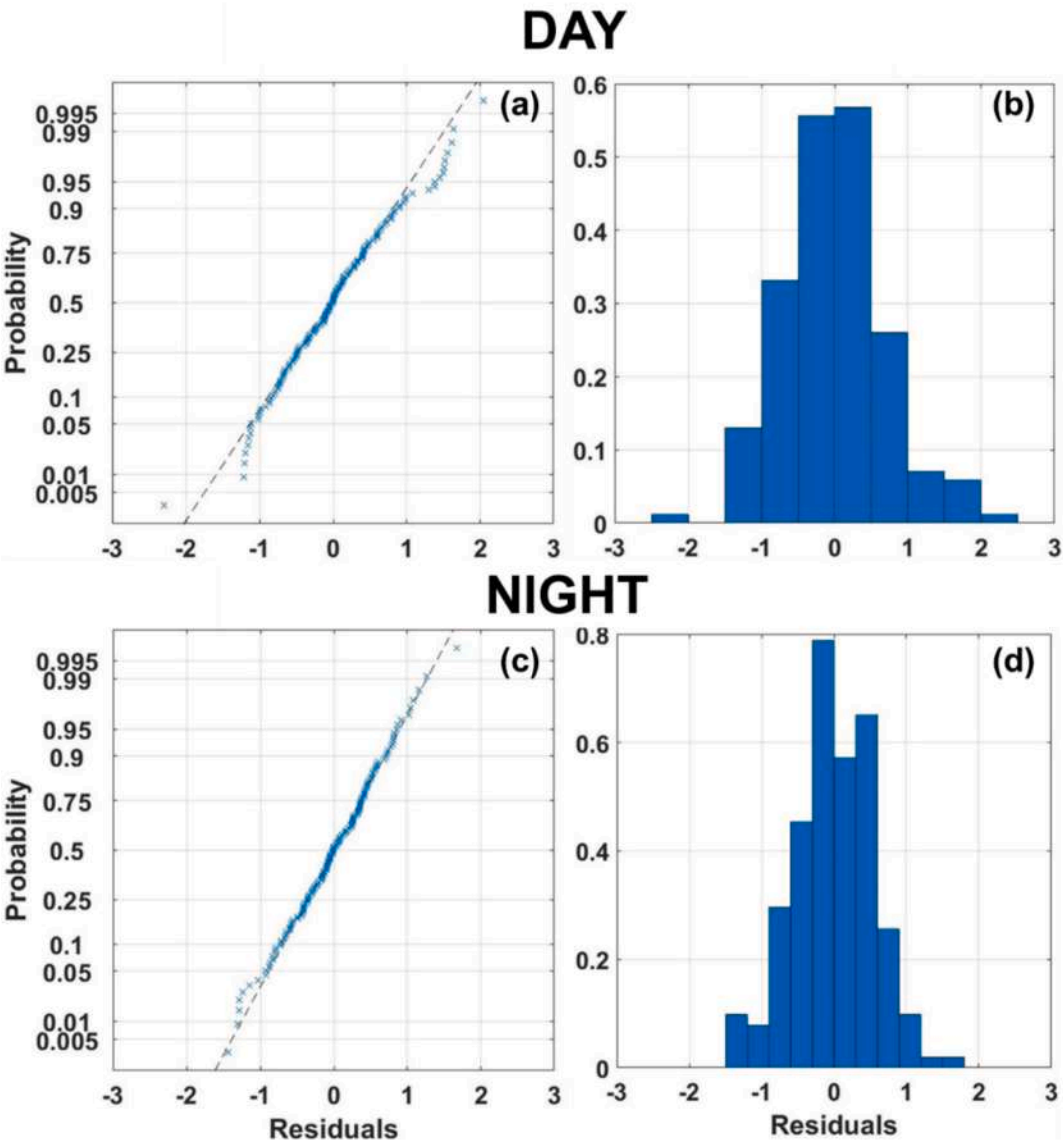


**Fig. 9.** As in Fig. 8, but for Lecce-Bari model.

MOD1 shows better overall fitting, particularly at night, while MOD2 performs well in some daytime scenarios, especially where MOD1 tends to overpredict. These findings underline the trade-off between local accuracy (MOD1) and broader generalization (MOD2) and suggest that the effectiveness of each model depends on both the time of day and the specific urban context. To further clarify the intended scope of application, it should be noted that the two generalized models (MOD2), one developed for Milan-Turin

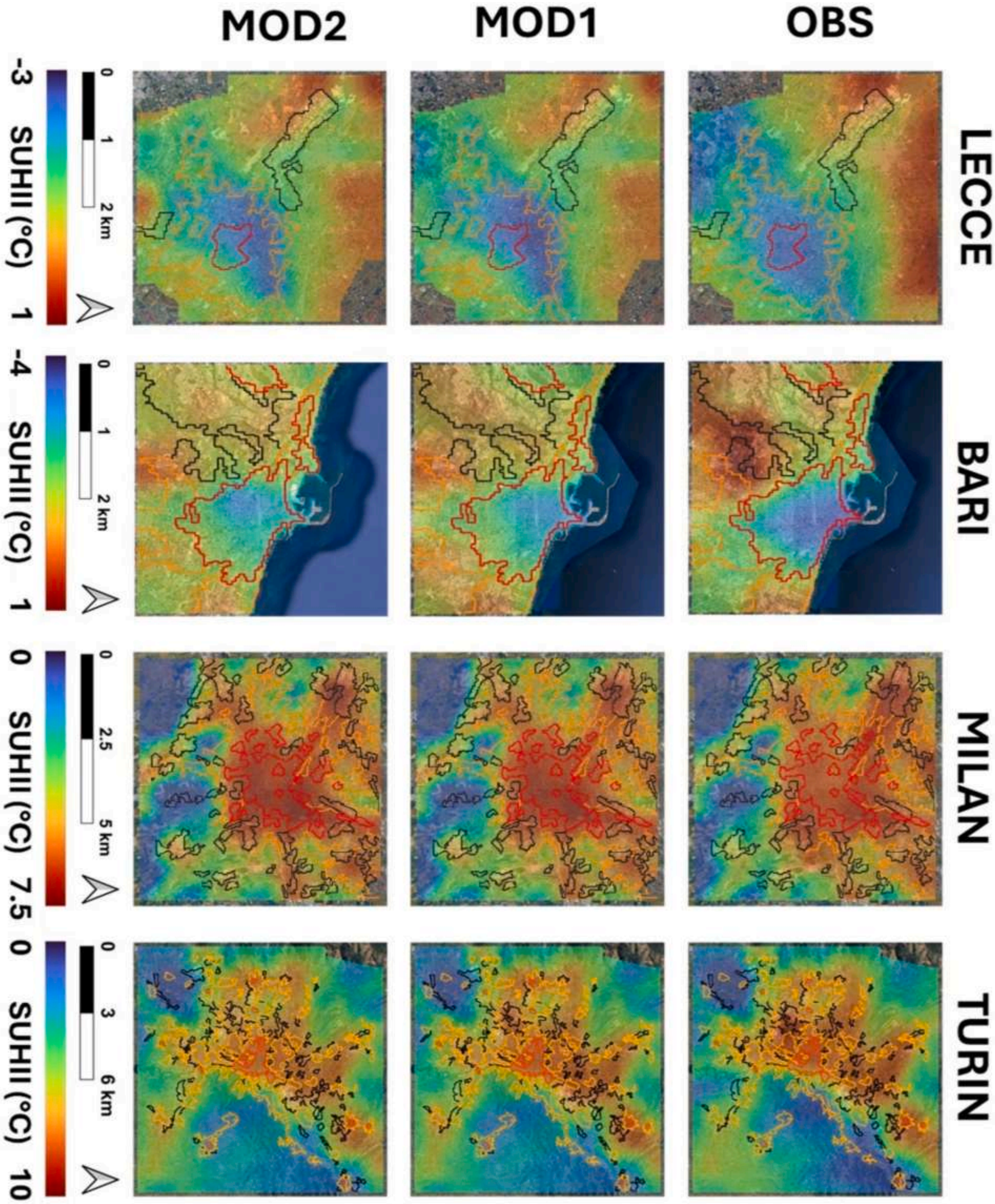


**Fig. 10.** Comparison between observed data (OBS) and model outputs (MOD1 and MOD2) during daytime for all the cities. Contour lines indicate the three main CLC classes (CLC 1, 2, 3).

and the other for Lecce-Bari, were conceptualised as regional models representative of distinct climatic and urban contexts. These models are primarily designed for multi-site analysis in similar environmental and morphological contexts but can also serve as transferable frameworks for preliminary assessments in other cities that share comparable climatic conditions and urban forms. In

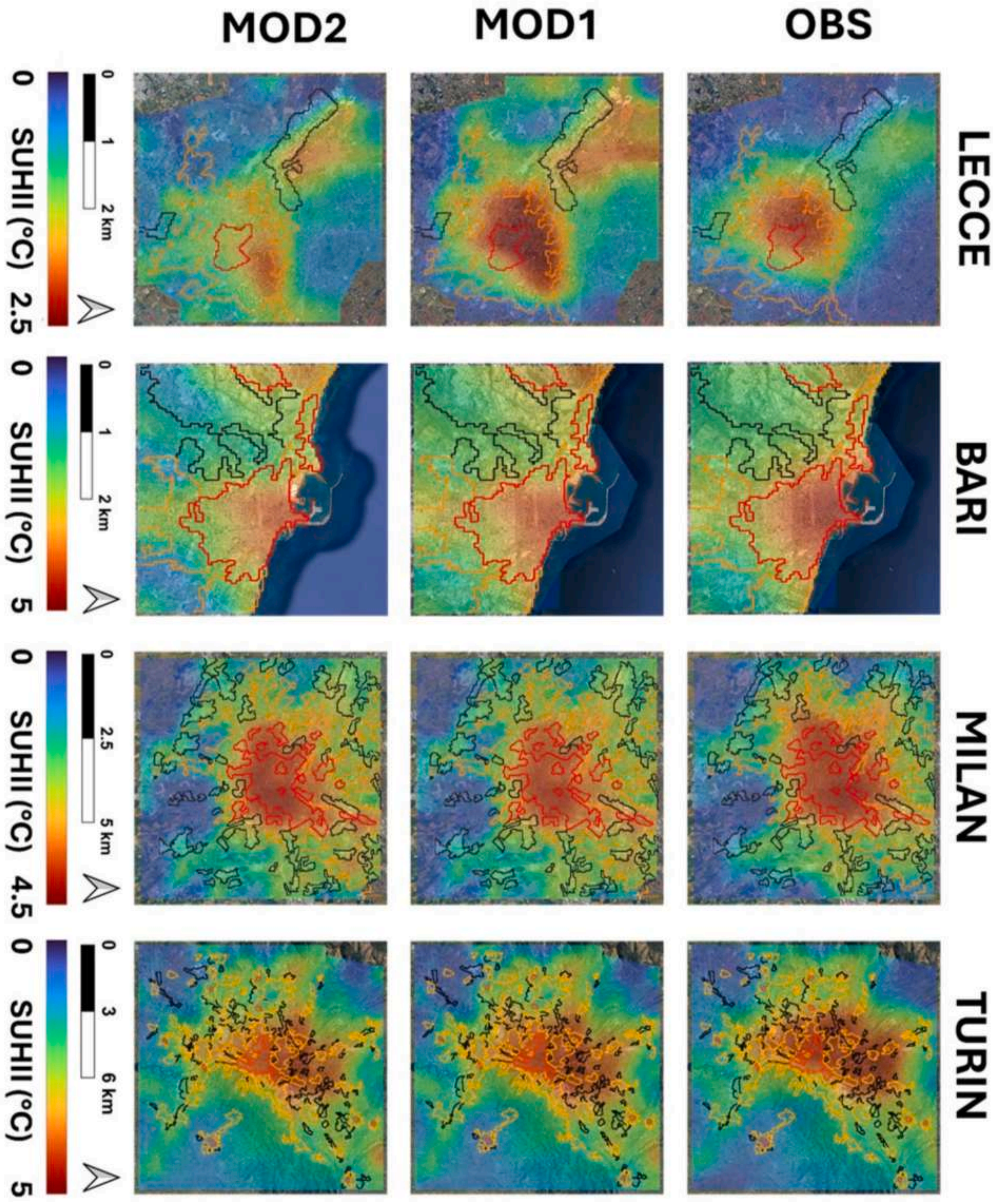


**Fig. 11.** As Fig. 10 but during nighttime.

**Table 12**
Mean difference (expressed in °C) between model outputs and observed data (MOD1-OBS and MOD2-OBS) for the three main CLC classes (CLC_1, CLC_2, and CLC_3).

| | CLC 1 | | CLC 2 | | CLC 3 | |
|---|---|---|---|---|---|---|
| | MOD1-OBS | MOD2-OBS | MOD1-OBS | MOD2-OBS | MOD1-OBS | MOD2-OBS |
| **DAY** | | | | | | |
| LECCE | 0.69 | 0.48 | 0.20 | 0.25 | 0.02 | −0.12 |
| BARI | −0.002 | 0.14 | −0.003 | 0.03 | −0.18 | −0.14 |
| MILAN | −0.06 | 0.09 | −0.10 | 0.04 | 0.001 | 0.09 |
| TURIN | 0.02 | −0.09 | 0.20 | 0.10 | −0.03 | −0.14 |
| NIGHT | | | | | | |
| LECCE | −0.09 | −0.32 | −0.03 | −0.05 | 0.06 | 0.27 |
| BARI | −0.19 | −0.77 | −0.33 | −0.81 | 0.07 | −0.32 |
| MILAN | −0.19 | −0.06 | 0.16 | 0.23 | 0.03 | 0.08 |
| TURIN | −0.005 | −0.14 | 0.04 | −0.03 | −0.10 | −0.17 |

contrast, city-specific models (MOD1) remain more appropriate for detailed local calibration and high-precision analysis where location-specific data are available.

### 3.5. Application of the model

Multiple linear regression models developed in this study were used as a predictive tool to assess SUHII. By modifying specific urban characteristics such as reducing the ISF through depaving, increasing vegetation cover (thereby enhancing LAI), or improving surface albedo using lighter or reflective materials, their respective impacts on SUHII can be quantitatively evaluated.

As a practical example, the city of Milan was analysed at a spatial resolution of 1 km × 1 km (Fig. 12). Within the study area, all grid cells with a BSF greater than 0.2 (representing the most central and densely built-up areas) were identified. In these areas, LAI and albedo values were increased by 0.5 and 0.03, respectively, but only when the original values were below the respective 25th percentile. These variations were applied consistently for both daytime and nighttime conditions.

Follow a schematic workflow of the model application referring to Fig. 4:

1. Identification of dense urban areas:

All grid cells with BSF > 0.2 were selected as representative of the most central and built-up portions of the city.

2. Parameter modification:

In these cells, LAI and α values were increased by +0.5 and + 0.03, respectively, but only where original values were below the respective 25th percentile.

3. Model recalculation:

The adjusted variables were reintroduced into the model equations to compute the new SUHII values under both daytime and nighttime conditions.

4. Comparison and evaluation:

The resulting SUHII maps were compared with the baseline scenario to quantify the cooling effect of the simulated interventions.

Figure 12 illustrates the effect of increased LAI and albedo on SUHII. The maps on the left show current conditions, while those on the right depict the simulated scenario after the implementation of the changes. A substantial reduction in SUHII is evident throughout the study area, where SUHII decreased by about 1.00 °C during both day and 0.75 °C during the night.

The observed surface temperature reductions underscore the efficacy of targeted urban greening and light-reflective materials in mitigating urban thermal stress. These results are in line with others published on the cooling effects of urban green infrastructure and reflective materials. For example, Guerri et al., 2021 showed that re-placing as little as 10 % of impervious surface with vegetated areas around industrial sites led to a 2.00 °C reduction in LST, confirming the high impact of relatively small-scale interventions. Similarly, Marando et al., 2022 reported that a minimum of 16 % increase in tree cover can produce an average urban temperature reduction of 1.00 °C in European cities, reinforcing the magnitude of the improvement observed in this study.

The consistency between the estimated SUHII reductions and findings reported in previous studies supports the validity of the modelling approach as a reliable and computationally efficient tool for evaluating the effectiveness of urban overheating mitigation strategies. Even modest, well-targeted interventions in vegetation and reflectivity can significantly enhance thermal comfort and resilience. Urban planning should prioritize densely built areas with limited greenery or low albedo, promoting nature-based solutions,

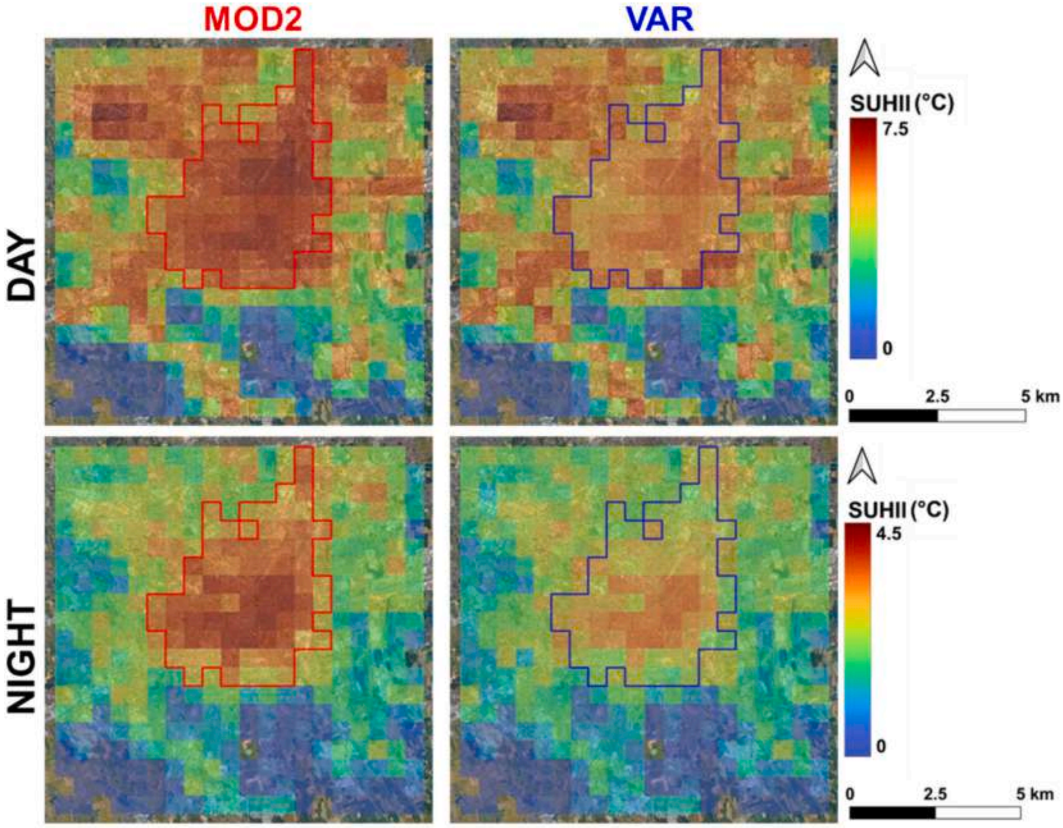


**Fig. 12.** Effect of albedo and LAI variation on SUHII intensity in Milan during daytime (up) and nighttime (bottom). The left maps represent the initial conditions, and the right maps show the impact of variation to urban characteristics. Highlighted in red and blue are areas with a BSF > 0.2. (For interpretation of the references to colour in this figure legend, the reader is referred to the web version of this article.)

green infrastructure, and reflective materials to improve climate adaptation and reduce heat-related health risks.

## 4. Conclusions

This study developed and applied a robust statistical modelling framework to assess the spatial and temporal variability of SUHII in four Italian cities (Lecce, Bari, Milan and Turin) by integrating urban morphological, land use and remote sensing data (summer months for 2022 and 2023). Results demonstrated significant intra- and inter-city differences in SUHII intensity. During daylight hours, Lecce and Bari showed predominantly negative or weakly positive SUHII values, consistent with patterns observed in arid or semi-arid environments, where soil moisture plays a crucial role. In contrast, Milan and Turin showed strongly positive daytime SUHII values, particularly in central urban and industrial areas, reflecting classic heat storage behaviour in temperate European cities. At night, all four cities recorded positive SUHII values, indicating heat retention, with Milan and Turin showing the highest intensities.

Multiple linear regression analyses, preceded by multicollinearity filtering using VIF, identified ISF, LAI and albedo as the most influential predictors of SUHII in all cities. ISF showed a positive association with nighttime SUHII, while LAI showed a strong negative influence in both daytime and nighttime, underscoring the cooling effects of urban greening. The albedo presented mixed effects depending on the time of day, suggesting interactions with surface material properties. HM showed a dual role, mitigating surface heat during the day mainly through shading but increasing SUHII at night due to reduced sky exposure and thermal inertia of built materials.

Regression diagnostics confirmed model validity, especially at night, with performance highest in Milan and Turin, moderate in Lecce, and lower in Bari for daytime conditions. Nighttime models consistently outperformed daytime ones. MDS and SIMPER analyses revealed two city clusters: Milan–Turin, with similar morphology and thermal behaviour, and Lecce–Bari, with greater internal variability. Generalized models for each cluster were statistically robust. Multicity models approximated city-specific performance well in northern cities by day but were less accurate at night in southern contexts.

Despite the promising results, this study has several limitations. First, the analysis was limited to the summer season and considered only two-time windows per day (late morning and early evening), thereby missing key daytime peaks and finer diurnal dynamics. Second, the spatial resolution of 1 km × 1 km, although suitable for city-scale comparisons, limits the ability to capture finer-scale urban heterogeneity. Future research could address this by applying downscaling techniques (e.g., statistical or sub-grid modelling) in combination with higher-resolution datasets such as LANDSAT or ECOSTRESS, to better capture fine-scale microclimatic variability within urban areas. Third, the focus on four cities, all within the Mediterranean-temperate climatic zones, restricts the generalizability of results to other climate regimes, such as tropical or continental environments. However, the regression models developed in this study could be applied to other cities with comparable morphological and climatic characteristics, provided that a careful validation is performed to ensure the robustness and reliability of the results.

Future work should aim to overcome these limitations by extending the analysis across multiple seasons and incorporating higher temporal frequency (e.g., including daytime peaks and nighttime minimum), as well as higher spatial resolution data. Expanding the city sample to include urban areas with diverse geometries, climates, and developmental contexts would enhance the model's transferability. Furthermore, integrating detailed datasets that describe the radiative and thermal properties of urban surfaces would allow for isolating the individual effects of specific mitigation strategies (e.g., cool roofs, vegetation). Additionally, incorporating satellite data from sensors like MODIS or ECOSTRESS would improve the characterization of SUHII by capturing its full diurnal variability, thereby allowing for a more detailed and dynamic analysis of the phenomenon.

This framework provides a flexible and scalable tool for assessing SUHII at different spatial and temporal scales, supporting both detailed local assessments and broader comparative studies. Its application can inform the design of context-specific mitigation policies, contributing to more effective and sustainable urban heat management.

## CRediT authorship contribution statement

**Antonio Esposito:** Writing – original draft, Validation, Software, Methodology, Investigation, Formal analysis, Data curation, Conceptualization. **Gianluca Pappaccogli:** Writing – review & editing, Writing – original draft, Supervision, Software, Methodology, Investigation, Conceptualization. **Fabio Bozzeda:** Writing – review & editing, Visualization, Validation, Methodology. **Riccardo Buccolieri:** Writing – review & editing, Visualization, Supervision, Resources, Project administration.

## Declaration of competing interest

The authors declare that they have no known competing financial interests or personal relationships that could have appeared to influence the work reported in this paper.

## Acknowledgements

This work is supported by: Progetto "RETE - Resilience of the Electric Transmission grid to Extreme events" (PNRR innovation grants) (CUP F83C22000740001); and by ICSC – Centro Nazionale di Ricerca in High Performance Computing, Big Data and Quantum Computing, funded by European Union – NextGenerationEU (CUP F83C22000740001). FB was funded from NBFC – National Biodiversity Future Center, funded by European Union – NextGenerationEU, Project code CN_00000033, CUP F87G22000290.

The authors acknowledge Eng. Giuseppe Maffeis from TerrAria S.r.l. for useful discussion.

## Data availability

Data will be made available on request.

## References

Albini, G., Guerri, G., Munafò, M., Morabito, M., 2025. Investigation of the surface urban Heat Island (SUHI) by two remote sensing-based approaches in Italian regional capitals. Remote Sens. Appl. Soc. Environ. 38, 101567. https://doi.org/10.1016/j.rsase.2025.101567.

Anniballe, R., Bonafoni, S., Pichierri, M., 2014. Spatial and temporal trends of the surface and air heat island over Milan using MODIS data. Remote Sens. Environ. 150, 163–171.

Bakker, J.D., 2024. Applied Multivariate Statistics in R. University of Washington, Seattle, p. 555.

Barker, L.E., Shaw, K.M., 2015. Best (but oft-forgotten) practices: checking assumptions concerning regression residuals. Am. J. Clin. Nutr. 102, 533–539. https://doi.org/10.3945/ajcn.115.113498.

Breusch, T.S., Pagan, A.R., 1979. A simple test for heteroscedasticity and random coefficient variation. Econometrica 47, 1287–1294. https://doi.org/10.2307/1911963.

Clinton, N., Gong, P., 2013. MODIS detected surface urban heat islands and sinks: global locations and controls. Remote Sens. Environ. 134, 294–304.

Deilami, K., Kamruzzaman, M., Liu, Y., 2018. Urban heat island effect: a systematic review of spatio-temporal factors, data, methods, and mitigation measures. Int. J. Appl. Earth Obs. Geoinf. 67, 30–42.

Deng, Y., Chen, R., Xie, Y., Xu, J., Yang, J., Liao, W., 2021. Exploring the impacts and temporal variations of different building roof types on surface urban heat island. Remote Sens. 13, 2840. https://doi.org/10.3390/rs13142840.

Donateo, A., Palusci, O., Pappaccogli, G., Esposito, A., Martilli, A., Santiago, J.L., Buccolieri, R., 2023. Analysis of urban heat island and human thermal comfort in a Mediterranean city: a case study of Lecce (Italy). Sustain. Cities Soc. 98, 104849. https://doi.org/10.1016/j.scs.2023.104849.

Durbin, J., Watson, G.S., 1950. Testing for serial correlation in least squares regression: I. Biometrika 37, 409–428. https://doi.org/10.1093/biomet/37.3-4.409.

Esposito, A., Grulois, M., Pappaccogli, G., Palusci, O., Donateo, A., Salizzoni, P., Santiago, J.L., Martilli, A., Maffeis, G., Buccolieri, R., 2023. On the calculation of urban morphological parameters using GIS: an application to Italian cities. Atmosphere 14, 329.

Esposito, A., Pappaccogli, G., Donateo, A., Salizzoni, P., Maffeis, G., Semeraro, T., Santiago, J.L., Buccolieri, R., 2024. Urban morphology and surface urban heat island relationship during heat waves: a study of Milan and Lecce (Italy). Remote Sens. 16 (23), 4496. https://doi.org/10.3390/rs16234496.

Garzón, J., Molina, I., Velasco, J., Calabia, A., 2021. A remote sensing approach for surface urban heat island modeling in a tropical Colombian city using regression analysis and machine learning algorithms. Remote Sens. 13, 4256. https://doi.org/10.3390/rs13214256.

Gelman, A., Hill, J., 2006. Data Analysis Using Regression and Multilevel/Hierarchical Models. Cambridge University Press, Cambridge.

Grimmond, C.S.B., Blackett, M., Best, M.J., Barlow, J., Baik, J.-J., Belcher, S.E., Bohnenstengel, S.I., Calmet, I., Chen, F., Dandou, A., Fortuniak, K., Gouvea, M.L., Hamdi, R., Hendry, M., Kawai, T., Kawamoto, Y., Kondo, H., Krayenhoff, E.S., Lee, S.-H., Loridan, T., 2010. The international urban energy balance models comparison project: first results from phase 1. J. Appl. Meteorol. Climatol. 49, 1268–1292. https://doi.org/10.1175/2010JAMC2354.1.

Guerri, G., Crisci, A., Congedo, L., Munafò, M., Morabito, M., 2021. A functional seasonal thermal hot-spot classification: focus on industrial sites. Sci. Total Environ. 806, 151383.

Heaviside, C., Macintyre, H., Vardoulakis, S., 2017. The urban heat island: implications for health in a changing environment. Curr. Environ. Health Rep. 4 (3), 296–305. https://doi.org/10.1007/s40572-017-0150-3.

IPCC, 2022. Climate Change 2022: Impacts, Adaptation, and Vulnerability. Contribution of Working Group II to the Sixth Assessment Report of the Intergovernmental Panel on Climate Change. Cambridge University Press, Cambridge, UK and New York, NY, USA. https://doi.org/10.1017/9781009325844.

Jeng, C.C., 2023. Why a variance inflation factor of 10 is not an ideal cutoff for multicollinearity diagnostics. J. Educ. Stud. 57 (2), 67–93.

Kutner, M.H., Nachtsheim, C.J., Neter, J., 2004. Applied Linear Regression Models, 4th ed. McGraw-Hill/Irwin, New York, NY, USA.

Liu, Y., Liu, B., 2022. Residual analysis and parameter estimation of uncertain differential equations. Fuzzy Optim. Decis. Making 21, 513–530. https://doi.org/10.1007/s10700-021-09379-4.

Marando, F., Heris, M.P., Zulian, G., Udías, A., Mentaschi, L., Chrysoulakis, N., Parastatidis, D., Maes, J., 2022. Urban heat island mitigation by green infrastructure in European functional urban areas. Sustain. Cities Soc. 77, 103564.

Martilli, A., Sanchez, B., Rasilla, D., Pappaccogli, G., Allende, F., Martin, F., Roman, C., Yagüe, C., Fernandez, F., 2021. Simulating the meteorology during persistent wintertime thermal inversions over urban areas: the case of Madrid. Atmos. Res. 263, 105789. https://doi.org/10.1016/j.atmosres.2021.105789.

Massey, F.J., 1951. The Kolmogorov–Smirnov Test for Goodness of Fit. J. Am. Stat. Assoc. 46, 68–78. https://doi.org/10.1080/01621459.1951.10500769.

Mead, A., 1992. Review of the development of multidimensional scaling methods. J. R. Stat. Soc. Series D 41 (1), 27–39.

Milelli, M., Bassani, F., Garbero, V., Poggi, D., Hardenberg, J., Ridolfi, L., 2023. Characterization of the urban heat and dry island effects in the Turin metropolitan area. Urban Clim. 47, 101397.

Mirzaei, P.A., Haghighat, F., 2010. Approaches to study urban Heat Island—abilities and limitations. Build. Environ. 45 (10), 2192–2201.

O'Brien, R.M., 2007. A caution regarding rules of thumb for variance inflation factors. Qual. Quant. 41 (5), 673–690.

Oukawa, G.Y., Krecl, P., Targino, A.C., 2022. Fine-scale modeling of the urban Heat Island: a comparison of multiple linear regression and random Forest approaches. Sci. Total Environ. 815, 152836. https://doi.org/10.1016/j.scitotenv.2021.152836.

Pappaccogli, G., Giovannini, L., Zardi, D., Martilli, A., 2020. Sensitivity analysis of urban microclimatic conditions and building energy consumption on urban parameters by means of idealized numerical simulations. Urban Clim. 34, 100677. https://doi.org/10.1016/j.uclim.2020.100677.

Pappaccogli, G., Giovannini, L., Zardi, D., Martilli, A., 2021. Assessing the ability of WRF-BEP+BEM in reproducing the wintertime building energy consumption of an Italian Alpine city. J. Geophys. Res. Atmos. 126, e2020JD033652. https://doi.org/10.1029/2020JD033652.

Pappaccogli, G., Esposito, A., Buccolieri, R., 2025. Summer diurnal LST variability across local climate zones using ECOSTRESS data in Lecce and Milan. Atmosphere 16, 377.

Pierri, C., Longo, C., Giangrande, A., 2010. Variability of fouling communities in the mar piccolo of Taranto (northern Ionian Sea, Mediterranean Sea). J. Mar. Biol. Assoc. UK 90, 159–167.

Rajeswari, J.R., Fountoukis, C., Siddique, A., et al., 2024. Urban heat island phenomenon in a desert, coastal city: the impact of urbanization. Urban Clim. 56, 102016.

Rallis, I., Chatzigeorgiou, G., Florido, M., et al., 2022. Early succession patterns of benthic assemblages on artificial reefs in the oligotrophic eastern Mediterranean Basin. J. Mar. Sci. Eng. 10, 620.

Rasul, A., Balzter, H., Smith, C., 2015. Spatial variation of the daytime surface urban cool island during the dry season in Erbil, Iraqi Kurdistan, from Landsat 8. Urban Clim. 14, 176–186.

Roy, T.B., Middey, A., Krupadam, R.J., 2025. Unveiling the microclimate: a comprehensive review of tools, techniques, and future directions for sustainable cities. Build. Environ. 274, 112726. https://doi.org/10.1016/j.buildenv.2025.112726.

Rydin, Y., Bleahu, A., Davies, M., Dávila, J.D., Friel, S., De Grandis, G., et al., 2012. Shaping cities for health: complexity and the planning of urban environments in the 21st century. Lancet 379 (9831), 2079–2108.

Saito, K., Ogawa, S., Aihara, M., Otowa, K., 2001. Estimation of LAI and forest management on Okutama. In: Proceedings of the 22nd Asian Conference on Remote Sensing, Singapore, 5–7 November, pp. 11–17.

Salmerón, R., García, C.B., García, J., 2018. Variance inflation factor and condition number in multiple linear regression. J. Stat. Comput. Simul. 88 (12), 2365–2384. https://doi.org/10.1080/00949655.2018.1463376.

Santamouris, M., Cartalis, C., Synnefa, A., Kolokotsa, D., 2015. On the impact of urban heat island and global warming on the power demand and electricity consumption of buildings—a review. Energ. Buildings 98, 119–124.

Schwarz, N., Schlink, U., Franck, U., Großmann, K., 2012. Relationship of land surface and air temperatures and its implications for quantifying urban heat island indicators—an application for the city of Leipzig (Germany). Ecol. Indic. 18, 693–704.

Shi, Y., Xiang, Y., Zhang, Y., 2019. Urban design factors influencing surface urban heat island in the high-density city of Guangzhou based on the local climate zone. Sensors 19, 3459. https://doi.org/10.3390/s19163459.

Stewart, I.D., Oke, T.R., 2012. Local climate zones for urban temperature studies. Bull. Am. Meteorol. Soc. 93, 1879–1900.

Sturrock, K., Rocha, J., 2000. A multidimensional scaling stress evaluation table. Field Methods 12, 49–60.

Sureiman, O., Mangera, C.M., 2020. F-test of overall significance in regression analysis simplified. J. Pract. Cardiovasc. Sci. 6 (2), 116–122. https://doi.org/10.4103/jpcs.jpcs_18_20.

World Meteorological Organization (WMO), 2025. Essential Climate Variables. https://gcos.wmo.int/site/global-climate-observing-system-gcos/essential-climate-variables (accessed 19 June 2025).

Yuan, F., Bauer, M.E., 2007. Comparison of impervious surface area and normalized difference vegetation index as indicators of surface urban Heat Island effects in Landsat imagery. Remote Sens. Environ. 106, 375–386.

Zhang, T., Zhou, Y., Zhu, Z., Li, X., Asrar, G.R., 2022a. A global seamless 1 km resolution daily land surface temperature dataset (2003−2020). Earth Syst. Sci. Data 14, 651–664. https://doi.org/10.5194/essd-14-651-2022.

Zhang, Y., Wang, Y., Ding, N., Yang, X., 2022b. Spatial pattern impact of impervious surface density on urban Heat Island effect: a case study in Xuzhou, China. Land 11, 2135. https://doi.org/10.3390/land11122135.

Zheng, Y., Li, Y., Hou, H., Murayama, Y., Wang, R., Hu, T., 2021. Quantifying the cooling effect and scale of large inner-city lakes based on landscape patterns: a case study of Hangzhou and Nanjing. Remote Sens. 13, 1526. https://doi.org/10.3390/rs13081526.

Zhou, D., Xiao, J., Bonafoni, S., Berger, C., Deilami, K., Zhou, Y., Frolking, S., Yao, R., Qiao, Z., Sobrino, J., 2019. Satellite remote sensing of surface urban heat islands: progress, challenges, and perspectives. Remote Sens. 11 (1), 48.